

1 **National-Scale Flood Risk Assessment Using GIS and Remote Sensing-**
2 **Based Hybridized Deep Neural Network and Fuzzy Analytic Hierarchy**
3 **Process Models: A Case of Bangladesh**

4
5 Zakaria Shams Siam^{a,e}, Rubyat Tasnuva Hasan^a, Soumik Sarker Anik^a, Fahima
6 Noor^a, Mohammed Sarfaraz Gani Adnan^{b,d}*, Rashedur M. Rahman^a, Ashraf
7 Dewan^c

8
9 *^a Department of Electrical and Computer Engineering, North South University, Dhaka,*
10 *Bangladesh*

11 *^b Department of Urban and Regional Planning, Chittagong University of Engineering and*
12 *Technology (CUET), Chattogram 4349, Bangladesh*

13 *^c Spatial Sciences Discipline, School of Earth and Planetary Sciences, Curtin University,*
14 *Perth 6102, Australia*

15 *^d Environment Change Institute, School of Geography and the Environment, University of*
16 *Oxford, OX1 3QY, United Kingdom*

17 *^e Department of Electrical and Computer Engineering, Presidency University, Dhaka,*
18 *Bangladesh*

19
20 * Corresponding author at: Mohammed Sarfaraz Gani Adnan; Department of Urban and
21 Regional Planning, Chittagong University of Engineering and Technology (CUET),
22 Chattogram 4349, Bangladesh; sarfarazadnan@cuet.ac.bd

23
24
25 This is a peer-reviewed, author's accepted manuscript of the following research article: Siam,
26 Z. S., Hasan, R. T., Anik, S. S., Noor, F., Adnan, M. S. G., Rahman, R. M., & Dewan, A.
27 (2022). National-scale flood risk assessment using GIS and remote sensing-based hybridized
28 deep neural network and fuzzy analytic hierarchy process models: a case of
29 Bangladesh. *Geocarto International*, 37(26), 12119-12148.
30 <https://doi.org/10.1080/10106049.2022.2063411>

National-Scale Flood Risk Assessment Using GIS and Remote Sensing-Based Hybridized Deep Neural Network and Fuzzy Analytic Hierarchy Process: A Case of Bangladesh

Assessing flood risk is challenging due to complex interactions among flood susceptibility, hazard, exposure, and vulnerability parameters. This study presents a novel flood risk assessment framework by utilizing a hybridized deep neural network (DNN) and fuzzy analytic hierarchy process (AHP) models. Bangladesh was selected as a case study region, where limited studies examined flood risk at a national scale. The results exhibited that hybridized DNN and fuzzy AHP models can produce the most accurate flood risk map while comparing among 15 different models. About 20.45% of Bangladesh are at flood risk zones of moderate, high, and very high severity. The northeastern region, as well as areas adjacent to the Ganges–Brahmaputra–Meghna rivers, have high flood damage potential, where a significant number of people were affected during the 2020 flood event. The risk assessment framework developed in this study would help policymakers formulate a comprehensive flood risk management system.

Keywords: Flood Risk Assessment; Flood Susceptibility Mapping; Hybridized Deep Neural Network; Hybridized Support Vector Regression; Genetic Algorithm; Fuzzy Analytic Hierarchy Process; Random Forest

Introduction

Flooding is known to be one of the most common yet devastating natural hazards (Stefanidis and Stathis 2013, Dewan 2015, Rahmati et al. 2020). Floods caused direct economic losses of USD 386 billion worldwide since 2001 (Wang et al. 2011, Rahmati et al. 2020). Economic damages caused by floods negatively impact human wellbeing, promoting long-term poverty in flood-affected regions (Adnan et al. 2020a, Barbour et al. 2022). An upsurge in population growth, exorbitant poverty, and climate change have increased flood risk in developing countries, especially in South Asia (Rahman et al. 2021a). Locating in an active deltaic region and crisscrossed by many large river channels, Bangladesh is frequently affected by floods of different magnitudes primarily due to high discharge in the Ganges, Brahmaputra, and Meghna (GBM) rivers caused by an excessive amount of rainfall in upstream regions (Chowdhury and Hassan 2017, Leon et al. 2020, Rahman et al. 2021b). The country is generally affected by four distinct types of floods: riverine or fluvial, flash or rainwater, urban or pluvial, and coastal floods (Adnan et al. 2019b). Heavy monsoon rainfall in the upstream river catchments leads to recurring riverine floods in Bangladesh (Rahman et al. 2021a). Various extreme riverine flood events, especially those that occurred in 1988, 1998, and 2004, killed many lives and caused extensive property damages, causing significant losses to the national economy (Dewan 2015). Most recently (in 2020), about a quarter of the country's lands was inundated by monsoon flooding, affecting over four million people (NASA 2020).

Since flooding is the outcome of extremely complex and intricate dynamic processes, it is nearly impossible to prevent it from occurring (Pappenberger et al. 2006). Hence, flood

75 risk reduction has become one of the major challenges worldwide (Rahmati et al. 2020).
 76 Reducing the detrimental effects of flooding depends on a quick and accurate assessment of
 77 risk, which helps to formulate risk management plans (Mojaddadi et al. 2017). The
 78 emergence of various remote sensing and the geospatial techniques has enabled researchers
 79 and practitioners to assess flood risk more accurately (Dewan and Kankam-Yeboah 2006,
 80 Pradhan 2010, Thirumurugan and Krishnaveni 2019, Rahman et al. 2021b). Evaluation of
 81 flood risk includes investigating flood risk-prone zones where the flood potentials are very
 82 high (Mojaddadi et al. 2017). A comprehensive flood risk assessment plays a vital role in the
 83 overall flood risk management system, which requires quantification of flood hazard,
 84 exposure, and vulnerability (Meyer et al. 2009, Pham et al. 2021a, Pham et al. 2021b).
 85 Various studies indicated that an accurate flood susceptibility model (FSM) can be translated
 86 into a flood hazard model by integrating factors such as flood depth, flood duration, and
 87 rainfall (Mojaddadi et al. 2017, Rahman et al. 2019, Pham et al. 2021a, Pham et al. 2021b,
 88 Rahman et al. 2021a).

89 Several studies conducted flood risk assessments both at the local and national scales
 90 around the world with the aid of remote sensing and GIS techniques, traditional statistical
 91 models, and multi-criteria decision analysis (MCDA) methods (Wang et al. 2011, Rincón et
 92 al. 2018, Luu et al. 2019, Akay and Baduna Koçyiğit 2020, Akay 2021, Ekmekcioğlu et al.
 93 2021). However, the results produced by those methods could be affected by the nonlinear
 94 and dynamic nature of flooding (Tehrany et al. 2015), scarcity of necessary data especially in
 95 developing countries (Darabi et al. 2019), and restricted applicability of the models at
 96 multiple scales (de Moel et al. 2015). The limitations of various statistical flood models have
 97 prompted researchers to apply different machine learning (ML) algorithms in assessing flood
 98 risk (Rahmati et al. 2020). Recent studies applied different standalone as well as hybridized
 99 ML models. For instance, hybridized support vector machine (SVM) (Mojaddadi et al. 2017,
 100 Ma et al. 2019b) including SVM based on the radial basis function (SVM-RBF) (Ngo et al.
 101 2021, Siam et al. 2021a) and SVM with the convolutional neural network (CNN) (Wang et
 102 al. 2020), standalone and hybridized decision table models (Pham et al. 2021b), hybridized
 103 decision tree (DT) (Chen et al. 2021) and others (Darabi et al. 2019). Tehrany et al. (2015)
 104 examined the efficacy of SVM in flood susceptibility mapping by comparing the
 105 performance of such models with four distinct kernels: linear, polynomial, RBF, and sigmoid.
 106 All these studies reported that hybridized ML models potentially produce more accurate
 107 results compared to standalone models (Rahmati et al. 2020, Siam et al. 2021a, Siam et al.
 108 2021b). Also, to address the uncertainties related to the classical MCDA approaches, a few
 109 studies exploited the fuzzy MCDA approach (Akay 2021, Costache et al. 2021, Vilasan and
 110 Kapse 2021).

111 The application of deep learning (DL) algorithms has proved to be very efficient in
 112 quantifying flood probability (Ma et al. 2019a). Recently, several studies have been
 113 conducted using various deep neural network (DNN) architectures for FSM, with various
 114 combinations of algorithms. The latest DNN-based flood susceptibility models include the
 115 use of (1) DNN in combination with the manta ray foraging optimization algorithm (Nguyen
 116 et al. 2021), (2) combined the multilayer perceptron (MLP) and autoencoder models
 117 (Ahmadlou et al. 2021), (3) CNN and recurrent neural network (RNN) (Panahi et al. 2021),

118 (4) standalone and hybridized CNN architectures (Wang et al. 2020). However, all these
119 studies were limited to flood susceptibility assessment. Consequently, little is known
120 regarding the applicability of hybridized models in assessing flood risk. Only a few studies
121 utilized DNN models (Chen et al. 2021) in combination with the MCDA approach for flood
122 risk modeling (Pham et al. 2021a, Pham et al. 2021b). Still, the use of the hybridized DNN
123 architectures is underexplored in flood risk studies. Besides, in the context of Bangladesh,
124 only a few studies carried out flood susceptibility assessment at a national scale (Rahman et
125 al. 2019, Rahman et al. 2021a, Rahman et al. 2021b, Siam et al. 2021a), while no study has
126 attempted to quantify country-level flood risk.

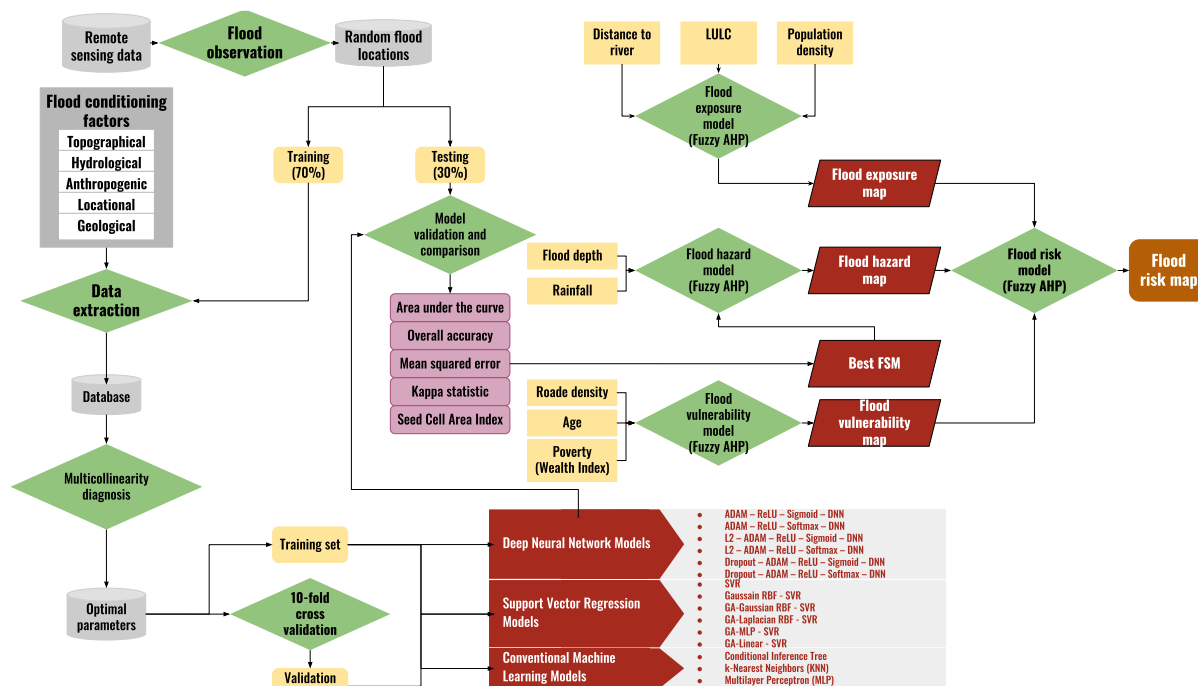
127 In response to the above-discussed research gaps, this study aims to present a flood
128 risk assessment framework by utilizing a hybridized DNN and fuzzy analytic hierarchy
129 process (AHP) models. This study hypothesized that the integration of hybridized DNN
130 model with the fuzzy AHP method can potentially produce more realistic results than the
131 classical AHP method. Unlike previous studies on risk assessment framework to flood, we
132 have modeled a hybridized DNN-based flood susceptibility model as a principal operator in
133 developing a flood hazard map. The framework has been applied in assessing flood risk at the
134 national scale in Bangladesh.

135

136 **Materials and methods**

137 The study was conducted in five steps. First, various flood conditioning factors were
138 identified for developing a flood susceptibility model. Second, flood susceptibility models
139 were developed based on different standalone and hybridized DNN and SVR models, as well
140 as other conventional ML models (e.g., conditional inference tree, KNN, and MLP). Third,
141 based on several evaluation metrics, the best-performing method was chosen for mapping the
142 flood susceptibility. Fourth, flood hazard, exposure, and vulnerability maps were developed
143 using the fuzzy AHP method, where the best-performing flood susceptibility map was used to
144 model flood hazards. Finally, a flood risk map was developed by integrating flood hazard,
145 exposure, and vulnerability maps. Figure 1 shows a brief methodological overview of the
146 present study.

147



148

149

Figure 1. Flowchart of this study

150

151

Study area

152

153

154

155

156

157

158

159

160

161

162

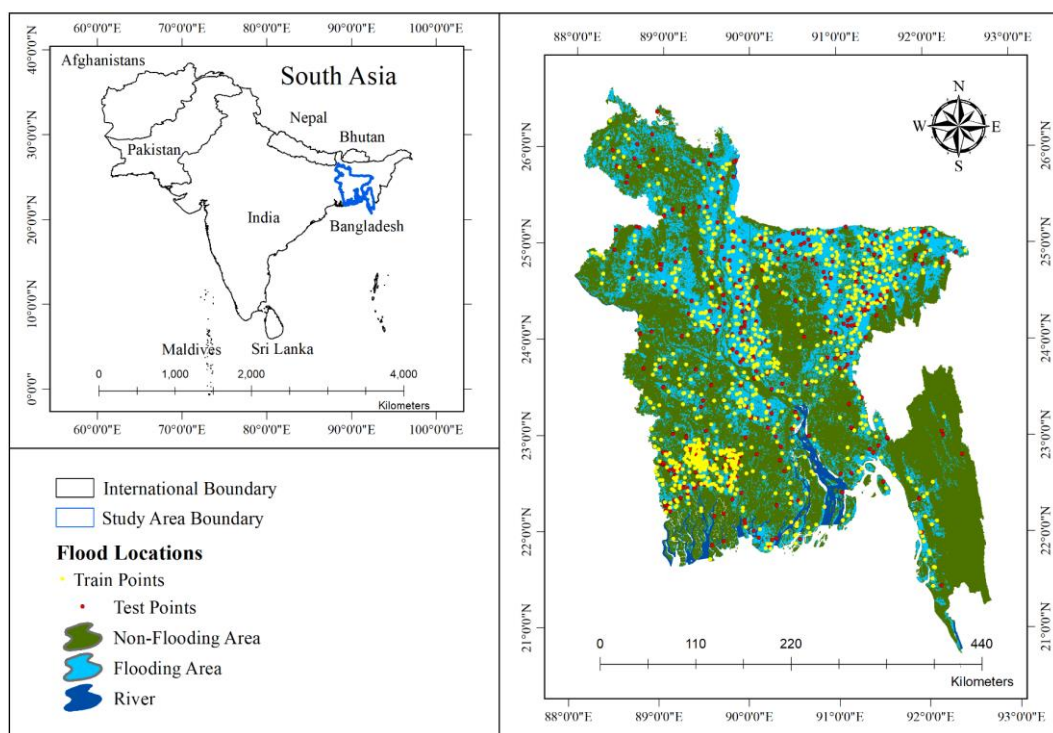
163

164

165

166

The present study focused on Bangladesh (Figure 2). Geographically, the country is located in South Asia, between the latitudes of 20°34' and 26°38' to the north and longitudes of 88°01' and 92°41' to the east (Hasan et al. 2017, Rahman et al. 2019). More than 162.7 million people inhabit the country, with an annual population growth rate of 1.37%, within an area of 1,47,570 km². Thus, Bangladesh has the highest population density in the world, with a density of approximately 1,063 people per km² (Hasan et al. 2017, Rahman et al. 2019). The country is characterized by five topographic regions — Chittagong, Tippera-Comilla, north Bengal, northeastern, and southwestern regions — comprising 64 districts, eight divisions, and 492 subdistricts (Islam and Sado 2000). It includes three major river systems: the Ganges, Meghna, and Brahmaputra, with numerous distributaries and tributaries. The geographical location, flat topography, and tropical climatic conditions of Bangladesh make it one of the world's most flood-prone areas. The yearly average precipitation generally ranges between 2200 and 2500 mm. Annual mean temperature ranges between 25 °C and 35 °C. Almost 80% of the total landmass of Bangladesh is fertile alluvial lowlands. The rest of the country slightly elevated older plains and small hilly regions (Rahman et al. 2019).



167
168 Figure 2. Map of Bangladesh with sample flood locations

169 ***Flood inventory mapping***

170 The flood inundation areas of historical flooding events are typically used as a dependent
171 variable for modeling flood susceptibility (Rahman et al. 2019, Pham et al. 2021a).
172 Inundation data, of three different periods (July 12-21, July 23-27, and July 29-August 02) in
173 monsoon season of 2020, were collected from the United Nations Institute for Training and
174 Research (UNITAR). The UNITAR used Sentinel-1 satellite data to detect inundated areas
175 (UNITAR 2020). The obtained inundation vector files were then converted to raster layers at
176 30 m resolution to ensure agreement with the digital elevation model (DEM) used in this
177 study. The inundation raster layer was binarized — non-flood and flood locations were
178 labeled as 0 and 1, respectively (equation 1).

$$Flood\ Inventory, y = \begin{cases} 1; & \text{if flooding} \\ 0; & \text{if non - flooding} \end{cases} \quad (1)$$

179 The combined flood inundation map was utilized to produce sample flood and non-
180 flood points. A total of 2,766 sample points (flood points – 1408 and non-flood points –
181 1358) were created using the stratified random sampling technique. The stratified random
182 sampling technique divides a population into smaller homogeneous subgroups known as
183 strata. The strata are constructed depending on the members' shared characteristics or
184 attributes. This technique has been widely used in flood modeling due to its ability to reduce
185 bias in the sample (Adnan et al. 2020a, Adnan et al. 2020b). Based on the previous studies
186 (Pham et al. 2021a, Pham et al. 2021b), the sample points were split into two groups: 70% of
187 the total sample points (983 flood points, 953 non-flood points) was considered to train the
188 flood susceptibility model while the other 30% sample (425 flood points, 405 non-flood
189 points) was employed to test the model. To reduce model overfitting, this study applied a 10-

190 fold cross-validation technique to further divide the train set (70% sample points) into train
191 and validation sets.

192

193 ***Flood conditioning factors***

194 An important component of preparing FSMs is to choose appropriate flood conditioning
195 factors that contribute to the occurrence of flooding in an area (Pham et al. 2021a). There is
196 no universal method to identify appropriate flood conditioning factors as different studies
197 used various combinations (Rahman et al. 2019, Wang et al. 2019, Costache et al. 2020a,
198 Rahmati et al. 2020, Talukdar et al. 2020, Pham et al. 2021a). However, factors should be
199 identified according to the environmental conditions of the study area (Adnan et al. 2020b).
200 In this study, initially, thirteen flood causative factors were chosen based on the
201 topographical, hydrological, locational, geological, and anthropogenic characteristics of the
202 study area. Selected factors include slope, aspect, curvature, elevation, Stream Power Index
203 (SPI), flow accumulation, Topographic Wetness Index (TWI), soil permeability, soil texture,
204 land use/land cover (LULC), geology, distance to rivers, and drainage density. The thematic
205 maps for all thirteen flood causative factors were developed at a spatial resolution of 30 m
206 (Figure 3).

207 Topographical factors considered for flood susceptibility modeling include elevation,
208 slope, aspect, and curvature. Surface elevation is an important factor accountable for flooding
209 (Bui et al. 2020a, Sarkar and Mondal 2020, Islam et al. 2021). Generally, elevation is
210 negatively associated with flooding, as areas with lower elevation tend to be highly
211 susceptible to flooding (Rahman et al. 2021b). In this study, a raster elevation layer was
212 prepared using the Advanced Land Observing Satellite (ALOS) Digital Elevation Model
213 (DEM) at 30 m resolution (JAXA 2015). Other topographical factors like slope, curvature,
214 and aspect are computed from DEM. Slope determines the runoff velocity after a rainfall
215 event (Talukdar et al. 2020). Flood potential is higher in areas with a lower slope and vice
216 versa (Adnan et al. 2020b). Aspect is another important topographical factor that indicates
217 slope directions (Adnan et al. 2020b). Generally, aspect denotes the magnitude of rainfall and
218 sunshine that an area would receive, influencing the water balance of an area (Tehrany et al.
219 2017). Curvature indicates geomorphological features of an area (Paul et al. 2019). Surfaces
220 with flat or concave characteristics are usually susceptible to flooding (Adnan et al. 2020b).

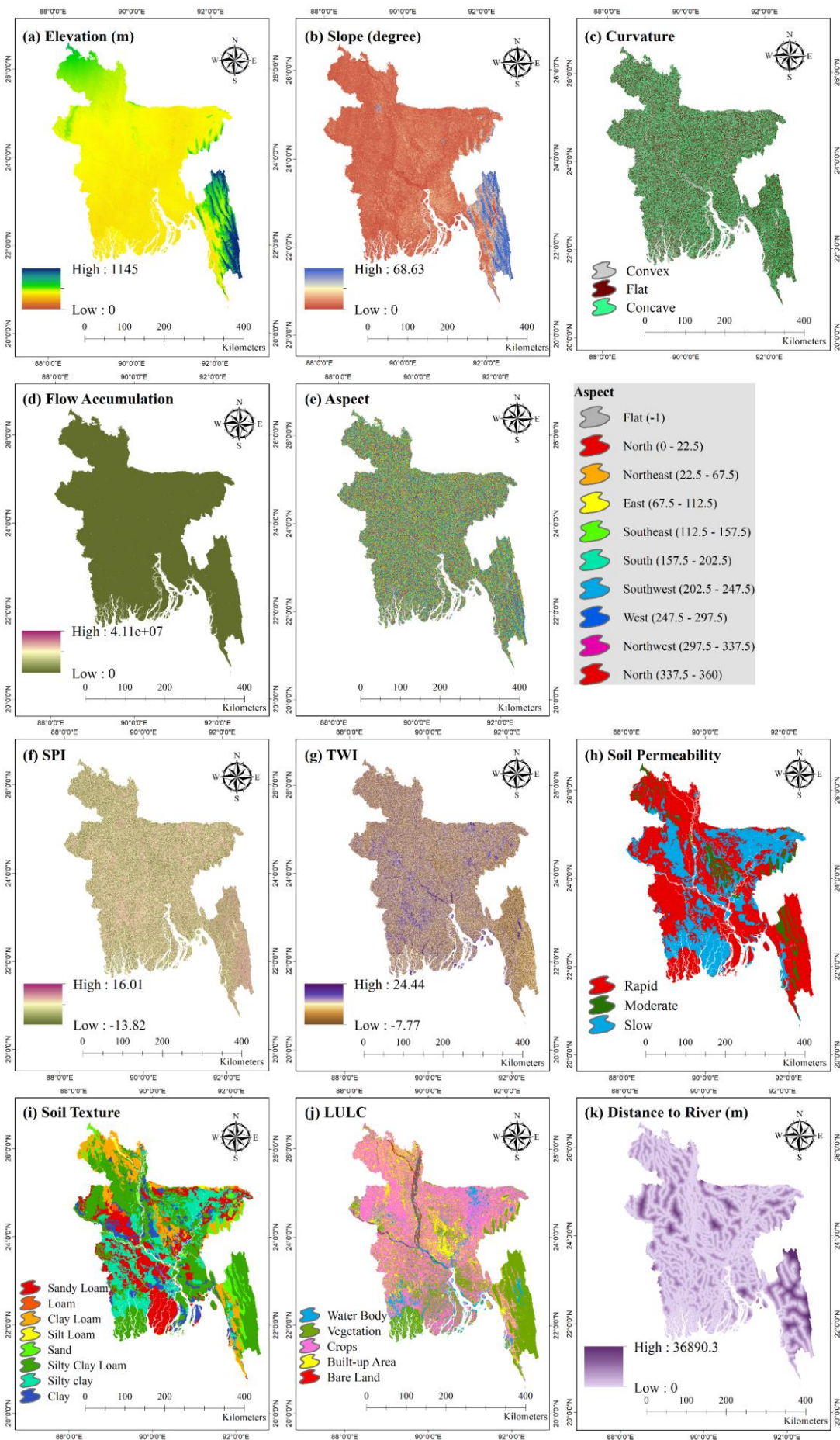
221 Flow accumulation is an important hydrological factor that impacts the flood
222 susceptibility of an area. The raster layer of flow accumulation was derived from DEM by
223 developing a continuing network of drainage systems (Planchon and Darboux 2002). Pixel-
224 wise flow accumulation value denotes accumulated water flowing in the downslope direction
225 (Adnan et al. 2020b). The flow accumulation layer was used to identify drainage channels
226 (Adnan et al. 2019a), which was later used to develop a drainage density layer. Other
227 hydrological factors such as SPI and TWI indicate drainage characteristics of the study area.
228 SPI typically exhibits the erosive power of flowing water (Talukdar et al. 2020), indicating
229 the rate of sediment that could relocate to natural drainage channels (Adnan et al. 2020b). On
230 the other hand, TWI denotes the amount of water that is accumulated in every pixel size
231 (Islam et al. 2021). TWI explains the possibility of a wet surface. An area with higher SPI

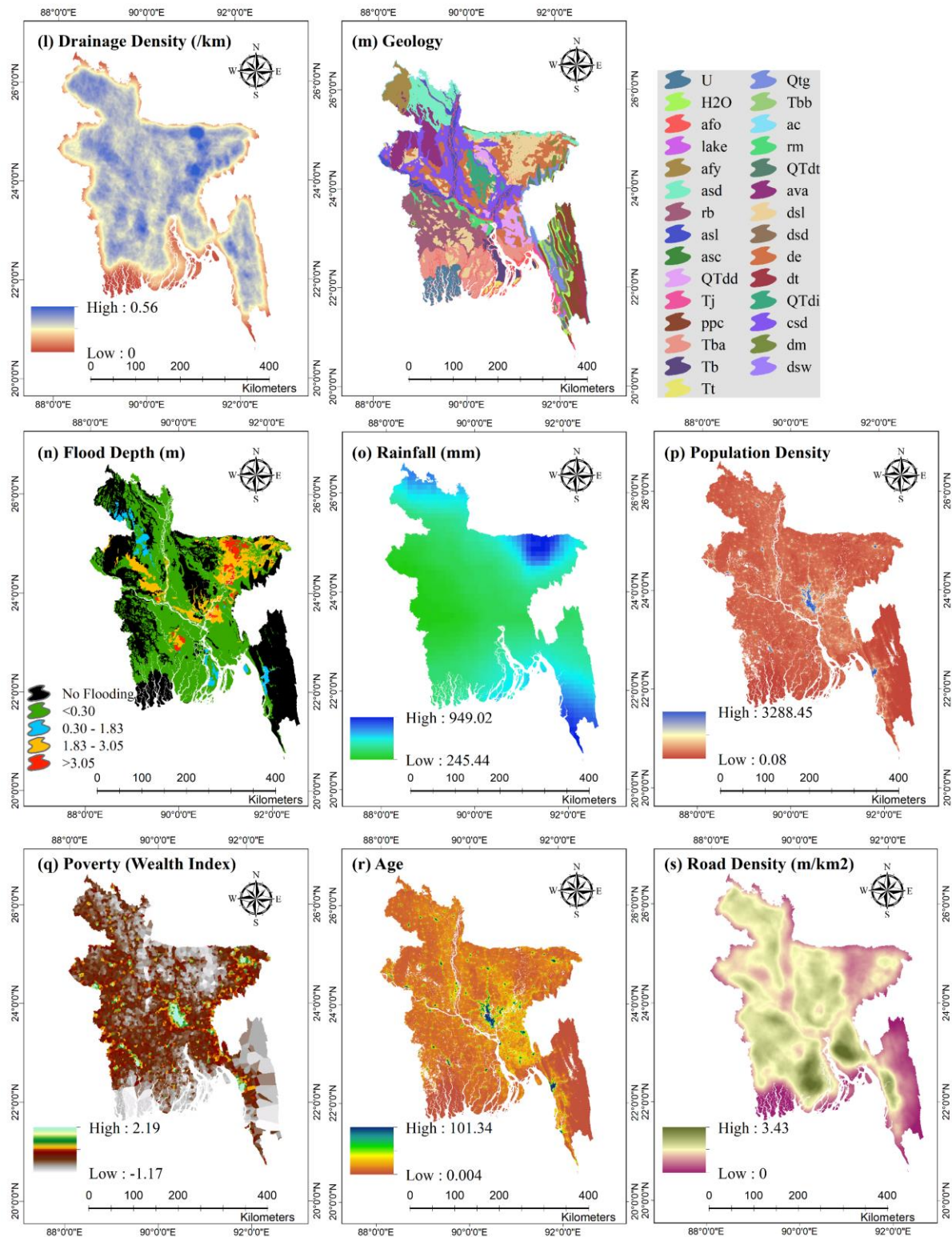
232 and TWI is highly likely to be flooded (Bannari et al. 2017). SPI and TWI were computed
 233 using equations (2) and (3).

$$SPI = A_s \times \tan\beta \quad (2)$$

$$TWI = \ln\left(\frac{A_s}{\beta}\right) \quad (3)$$

234 where, A_s is the fixed catchment region (m^2/m) and β is the slope gradient.





236

237 Figure 3. Thematic layers of various indicators for modeling flood risk

238 This study also used three geological factors: geology, soil permeability, and soil
 239 texture. Soil texture controls infiltration rate as well as surface runoff, hence, it is considered
 240 a significant flood conditioning factor (Rahman et al. 2021b). The raster layer of soil texture
 241 was taken from Bangladesh Agricultural Research Council (BARC) database (BARC 2014).

242 Soil permeability data can explain runoff patterns and drainage processes. It indicates the
 243 hydraulic activity of unsaturated soils and is an important factor influencing streamflow
 244 (Singh et al. 2020). The soil permeability data were also obtained from BARC (2014). This
 245 study also considered the geological characteristics of Bangladesh. The geology of an area
 246 influences the formation and construction of drainage patterns (Islam and Sado 2000, Bui et
 247 al. 2019), leading to the generation and development of floodplains. Typically, areas with a
 248 mostly impenetrable surface geology are highly susceptible to flood (Islam and Sado 2000).
 249 The digital geological data of Bangladesh was taken from the United States Geological
 250 Survey (USGS) (Persits et al. 2001).

251 LULC is a crucial flood conditioning factor since it directs the initiation as well as
 252 infiltration of the surface runoff and transportation of sediment (Adnan et al. 2020b). It
 253 directly impacts some parameters in the hydrological cycle such as interception and
 254 concentration (Rahman et al. 2019). Generally, built-up areas are more prone to flooding
 255 compared to the forest and open spaces due to low infiltration rates and high surface runoff
 256 (Talukdar et al. 2020). LULC data of 2020 was collected from the Environmental Systems
 257 Research Institute (Esri), which is developed using Sentinel-2 imagery (Karra et al. 2021).

258 Rivers are considered as the main paths of water flow causing flood events (Rahmati
 259 et al. 2020). This study incorporated a layer explaining distance to river as a locational factor
 260 (Mojaddadi et al. 2017). Areas that are close to the river are generally more susceptible
 261 (Costache et al. 2020b, Talukdar et al. 2020). The distance to river layer was derived from a
 262 river network database, collected from Water Resources Planning Organization (WARPO)
 263 (WARPO 2018) using the Euclidean distance algorithm. Table 1 shows a summary of the
 264 sources and spatial resolution of flood causative factors.

265
 266 Table 1. Indicators used for flood susceptibility, hazard, exposure and vulnerability modeling

No.	Factors	Spatial resolution	Variable type	Sources
1	Elevation	30 m	Numeric	(JAXA 2015)
2	Slope	"	Numeric	Derived from DEM
3	Aspect	"	Categorical	"
4	Curvature	"	Categorical	"
5	Flow Accumulation	"	Numeric	"
6	SPI	"	Numeric	"
7	TWI	"	Numeric	"
8	Soil Permeability	"	Categorical	(BARC 2014)
9	Soil Texture	"	Categorical	(BARC 2014)
10	LULC	10 m	Categorical	(Karra et al. 2021)
11	Geology	30 m	Categorical	(Persits et al. 2001)
12	Distance to River	"	Numeric	(WARPO 2018)
13	Drainage Density	"	Numeric	Derived from DEM
14	Flood Depth	"	Categorical	(BARC 2014)
15	Rainfall	11.1 km	Numeric	(Huffman et al. 2019)
16	Population Density	100 m	Numeric	(WorldPop 2020)

	(Population per Cell)			
17	Age (Less than 14 and Greater than 60)	100 m	Categorical	(Bondarenko et al. 2020)
18	Poverty (Wealth Index)	60 m – 5 km	Numeric	(Steele et al. 2017)
19	Road Density	30 m		(WARPO 2018)

267

268 ***Flood risk components***

269 *Flood hazard*

270 This study considered flood susceptibility (Pham et al. 2021a), flood depth (Pham et al.
 271 2021a), and rainfall (David and Schmalz 2020) to develop a flood hazard map of Bangladesh
 272 (Table 1). Rainfall is a crucial hydrological factor for flood hazard mapping (Lu et al. 2020).
 273 In Bangladesh, both short-term heavy rainfall and long-term low to moderate rainfall are
 274 accountable for flooding (Adnan et al. 2019b). Rainfall can cause hydrostatic pressure,
 275 promoting a higher water level in the major rivers (Rahman et al. 2019). Satellite-derived
 276 gridded precipitation data of July and August 2020, collected from Huffman et al. (2019),
 277 were used to develop a layer of the average monthly total rainfall. A thematic layer of flood
 278 depth was collected from BARC (2014) (Figure 3 (n)).

279

280 *Flood exposure*

281 Three indicators were used for developing a flood exposure map: distance to river, LULC,
 282 and population density (Table 1). Previous studies considered population density as an
 283 important indicator for modeling flood exposure (Zou et al. 2013, Pham et al. 2021a). Flood-
 284 prone areas with a high population density are more vulnerable to flooding than areas with a
 285 low density. In this study, population density data of 2020 was collected from WorldPop
 286 (2020) (Figure 3 (p)). As described in section 2.3, areas near the river are identified from
 287 DEM, and LULC data are collected from Karra et al. (2021).

288

289 *Flood vulnerability*

290 Flood vulnerability is typically correlated with the type of infrastructures as well as
 291 characteristics of the communities in flood-prone areas. Flood vulnerability was estimated
 292 based on three indicators: road density (Ronco et al. 2015, Pham et al. 2021a), age (Brito et
 293 al. 2018), and poverty (wealth index) (Pham et al. 2021a) (Table 1). Generally, flood-prone
 294 areas with a high road density are vulnerable to flooding (Pham et al. 2021a). A raster road
 295 density layer was derived from road network data collected from WARPO (2018). The
 296 population age structure is also a useful flood vulnerability indicator (Brito et al. 2018). A
 297 high percentage of children and older people increase flood vulnerability of an area (Brito et
 298 al. 2018). The age distribution data was retrieved from the WorldPop (Bondarenko et al.
 299 2020), where the total number of people aged less than 14 and greater than 60 was estimated
 300 for Bangladesh for the year 2020. Also, an area with a high poverty ratio becomes vulnerable
 301 to flooding (Adnan et al. 2020a, Pham et al. 2021a). The wealth index data was retrieved
 302 from Steele et al. (2017) to analyze poverty scenarios. Flood vulnerability indicator maps are
 303 shown in Figure 3 (q–s).

304

305 ***Flood risk assessment***

306 We estimated flood risk to be the product of flood hazard, exposure, and vulnerability
 307 (equation 4) (Pham et al. 2021a, Pham et al. 2021b).

$$Flood Risk = Flood Hazard \times Flood Exposure \times Flood Vulnerability \quad (4)$$

308
 309 ***Flood susceptibility modeling***

310 Flood susceptibility modeling was considered as a component of flood hazard mapping.
 311 Pixel-wise flood susceptibility scores (FS) were estimated using equation (5) (Rahman et al.
 312 2019, Siam et al. 2021a).

$$FS = \sum_{j=1}^n w_j x_j \quad (5)$$

313 where n denotes the number of flood conditioning factors used for FSM, x_j indicates
 314 selected flood conditioning factors and w_j represents the weight of every factor. To find the
 315 optimal weight of every factor for flood susceptibility modeling, a total of six standalone and
 316 hybridized DNN models were established: adaptive moment estimation (ADAM) – rectified
 317 linear unit (ReLU) – Softmax – DNN, ADAM – ReLU – Sigmoid – DNN, L2 regularization
 318 (L2) – ADAM – ReLU – Softmax – DNN, L2 – ADAM – ReLU – Sigmoid – DNN, Dropout
 319 – ADAM – ReLU – Softmax – DNN and Dropout – ADAM – ReLU – Sigmoid – DNN.

320 Also, a total of six standalone and hybridized SVR models were investigated such as
 321 standalone SVR, Gaussian Radial Basis Function Kernel (Gaussian RBF) – SVR using grid
 322 search technique, GA – Gaussian RBF – SVR, GA – laplacian RBF kernel (Laplacian RBF) –
 323 SVR, GA – sigmoid or multilayer perceptron kernel (MLP) – SVR and GA – linear kernel
 324 (Linear) – SVR. Besides, three conventional ML models (e.g., conditional inference tree, k-
 325 nearest neighbor (KNN), and MLP) were established. All standalone and hybridized deep
 326 neural network models were developed using the ‘keras’ package in the R programming
 327 language. The conditional inference tree, k-nearest neighbor, and multilayer perceptron
 328 models were established using the ‘ctree’ function of ‘party’ package, ‘knnreg’ function of
 329 ‘caret’ package, and ‘neuralnet’ function of ‘neuralnet’ package in R, respectively.

330 i. **Multicollinearity analysis for optimizing features**

331 In the present study, multicollinearity among flood causative factors was diagnosed by
 332 estimating the variance inflation factors (VIF) (Midi et al. 2010), using the ‘Car’ package in
 333 R, to remove factors that are subject to multicollinearity. VIF for each factor should be <2.5
 334 to circumvent the model bias (Midi et al. 2010). If the value is >10, it denotes the presence of
 335 multicollinearity (Midi et al. 2010). After investigating multicollinearity, the flood
 336 susceptibility model includes a total of eleven flood conditioning factors whose VIF values
 337 were less than 2.5 (Bai et al. 2011). TWI and flow accumulation layers were discarded since
 338 the addition of these two layers increased VIF values (Table 2).

339 Table 2. VIF values, indicating multicollinearity of selected factors

Factors	VIF (Iteration 1)	VIF (Iteration 2)
Aspect	1.029	1.007
Distance to River	1.162	1.160
Drainage Density	1.189	1.182
Elevation	2.496	2.472

Flow Accumulation	4.119	-
Geology	1.487	1.481
LULC	1.255	1.254
Curvature	1.251	1.182
Slope	3.673	1.833
Soil Permeability	1.997	1.988
Soil Texture	2.461	2.459
SPI	6.410	1.284
TWI	7.621	-

340

341 ii. Feature scaling

342 Since we exploited gradient descent as well as distance-based models, all continuous
 343 variables such as slope, drainage density, distance to river, elevation and SPI were scaled
 344 using z-score normalization technique (equation 6).

$$z = \frac{x - \mu}{\sigma} \quad (6)$$

345 where, x is the feature value, μ and σ are mean and standard deviation of that feature,
 346 respectively. After feature scaling, values of eleven flood conditioning factors were extracted
 347 corresponding to flood and non-flood points.

348

349 iii. Standalone and hybridized DNN models

350 We developed and applied six standalone and hybridized DNN models for mapping flood
 351 susceptibility. In the DNN model, we experimented with three hidden layers consistent with
 352 the study by Bui et al (Bui et al. 2019). A total of eleven nodes (i.e., 11 flood conditioning
 353 factors) were taken in the input layer and one node (sample flood points) in the output layer.
 354 We set the number of nodes to eight in each of the three consecutive hidden layers since the
 355 number of nodes in each hidden layer is suggested to be in between the number of input
 356 nodes and output nodes (Bui et al. 2020b). We used rectified linear activation function
 357 (ReLU) in each of the three hidden layers. However, in the output layer, we used the sigmoid
 358 activation function and the softmax activation function separately. For the sigmoid activation
 359 function, we used the binary cross-entropy loss function. For the softmax activation function,
 360 we applied one-hot encoded the output variable. Therefore, the number of output nodes
 361 became two instead of one in the case of the softmax activation function. For the loss
 362 function, we used the categorical cross-entropy function for the softmax activation function.

363 We initialized the weights setting the parameters of mean to 0, the standard deviation
 364 to 0.05, and the biases with the values of zero. For gradient descent optimization, we used the
 365 ADAM optimizer that integrates the gradient descent with momentum technique with the
 366 root mean square propagation (RMSprop) method. In the model, the number of epochs and
 367 mini-batches was set to 50 and 32, respectively. To circumvent the model overfitting issue
 368 with the train set, we further divided the train set (70% sample points) into train and
 369 validation sets implementing a 10-fold cross-validation technique so that the prediction
 370 accuracy on the test set (30% sample points) gets maximized.

371 We hybridized two DNN models: ADAM – ReLU – Sigmoid – DNN and ADAM –
 372 ReLU – Softmax – DNN, using two approaches that are L2 regularization and dropout

373 technique to reduce the high variance in the models. For L2 regularization, we specified
 374 regularization as the parameter in each of the three hidden layers and set the value of λ to
 375 0.001. For dropout, we added an extra layer after each of the three hidden layers and set the
 376 value of κ to 0.6.

377 iv. Standalone and hybridized SVR models

378 We developed and evaluated six standalone and hybridized SVR models for predicting flood
 379 susceptibility. First, the baseline SVR model was developed and combined with four different
 380 kernel functions (e.g., linear, gaussian RBF, laplacian RBF, and MLP kernels) separately.
 381 The grid search algorithm and GA were used for hyperparameter tuning and hybridization.

382 The objective of SVR is to generate function, describing correlation between input
 383 and output mentioned in equation (7).

$$f(x) = w^T \psi(x) + bias \quad (7)$$

384 where, $x \in R^n$ indicates flood conditioning features, $w \in R^n$ represents weight vector,
 385 and non-linear mapping function is denoted by $\psi(x)$. The final solution to the constrained
 386 optimization problem in SVR using Lagrangian formulation is described in equation (8).

$$f(x) = \sum_{j=1}^n (\alpha_j - \alpha_j^*) k(x, x_j) + bias \quad (8)$$

387 where, α_j and α_j^* denote the Lagrangian multipliers and $k(x_m, x_n) = <$
 388 $\psi(x_m), \psi(x_n) >$ indicates the kernel function. Various types of kernel functions could be
 389 employed (Rahmati et al. 2020). The linear, gaussian RBF, laplacian RBF and MLP kernels
 390 can be described in equations (9)-(12), respectively.

$$k(x, x_j) = sum(x, x_j) \quad (9)$$

$$k(x, x_j) = e^{-\gamma \|x-x_j\|^2} \quad (10)$$

$$k(x, x_j) = e^{-\frac{\|x-x_j\|}{\gamma}} \quad (11)$$

$$k(x, x_j) = tanh(Ax^T x_j + B) \quad (12)$$

391 where, γ is an optimizing hyperparameter indicating the spread of the kernel. A is the
 392 scale value and B is the offset value. The prediction accuracy of SVR model also depends on
 393 other parameters, that are, epsilon, ϵ representing approximation quality and the cost value
 394 that determines the tradeoff between model complexity and training error.

395 In the standalone SVR model, we have set epsilon to 0.1, cost to 1, and gamma to 0.1.
 396 For gaussian RBF – SVR, we optimized gamma and cost using the grid search technique in
 397 combination with the 10-fold cross-validation technique while setting epsilon to 0.1. We
 398 searched from 0.1 to 2 (interval = 0.1) to find the optimal value of gamma. The optimal value
 399 of cost was searched from 0.1 till 10 (interval = 0.1) using a grid search algorithm. This
 400 resulted in generating and training a total of 2000 SVR models with different values of
 401 gamma and cost. The optimal parameter values derived from the grid search technique
 402 produce the least mean squared error (MSE) on the test dataset. Using GA, we optimized the
 403 parameters of GA – Linear – SVR (i.e., epsilon and cost), GA – Gaussian RBF – SVR and
 404 GA – Laplacian RBF – SVR (i.e., epsilon, cost, and gamma), and GA – MLP – SVR (i.e.,
 405 epsilon, cost, scale, and offset). The negative quantity of the MSE on the test set prediction
 406 was defined as the objective function of GA as we maximized the objective function. Again,

407 a 10-fold cross-validation technique was employed while training all the SVR models on the
 408 train set to reduce overfitting.

409

410 v. Conventional ML models

411 This study also developed three conventional ML models: conditional inference tree, KNN,
 412 and MLP models. The conditional inference tree is a distinct type of decision tree model that
 413 employs recursive partitioning of the dependent variables depending on the correlation values
 414 to avoid biasing. This model exploits a significance test to choose the input variables rather
 415 than choosing the variable maximizing the information measure. We set the values of the
 416 minimum criterion and split to 0.95 and 200, respectively. KNN is a supervised ML model
 417 that assumes the similarity or resemblance between the novel case and the known or available
 418 cases and consequently puts the novel case into the class or category most similar to the
 419 available classes or categories (Costache et al. 2020a). We experimented with different
 420 values for k in the KNN model. However, the model performed better for a k value of five.
 421 MLP is another supervised ML model that provides a very fundamental feedforward neural
 422 network architecture utilized for both classification and regression-based problems
 423 (Ahmadlou et al. 2021). In the architecture of MLP, we used two hidden layers with the first
 424 layer containing a total of ten nodes and the second layer containing a total of three nodes.
 425 We set the values of the threshold to 0.1 and the maximum steps for training to 10^6 . We used
 426 RPROP+ as the learning algorithm for MLP.

427

428 vi. Validation and comparison of models

429 For identifying the best performing flood susceptibility model, this study estimated values of
 430 various cutoff-dependent and cutoff-independent validation indicators using the ‘roc’ and
 431 ‘plot.roc’ functions of ‘pROC’ package in R. The indices include receiver operating
 432 characteristic (ROC) and area under the receiver operating characteristic (AUROC) curves,
 433 kappa statistic, overall accuracy (OA), positive predictive value (PPV), negative predictive
 434 value (NPV), sensitivity, specificity, and MSE. We used Youden’s index for estimating the
 435 optimal cutoff point (Youden 1950) and binarized the predicted flood susceptibility scores by
 436 the models (Adnan et al. 2020b). We also estimated the seed cell area index (SCAI) (Akay
 437 2021) values for validation and comparison of flood susceptibility, hazard, exposure,
 438 vulnerability, and risk models.

439

440 vii. Flood susceptibility map

441 Applying the best-performing flood prediction model, a flood susceptibility map of
 442 Bangladesh was developed using the ArcGIS 10.8 software. The susceptibility values were
 443 normalized on a 0-1 scale. The resultant flood susceptibility map was categorized into five
 444 classes using the equal interval method in GIS: Very Low (0 – 0.2), Low (0.2 – 0.4), Medium
 445 (0.4 – 0.6), High (0.6 – 0.8), and Very High (0.8 – 1) (Rahman et al. 2019).

446

447 *Flood hazard modeling*

448 Flood hazard in the study area was estimated using equation (13) (Pham et al. 2021a, Pham et
 449 al. 2021b).

$$Flood\ Hazard\ Score = A_1 \times Flood\ Susceptibility\ Score + B_1 \times Flood\ Depth + C_1 \times Rainfall \quad (13)$$

450 where, A_1 , B_1 , and C_1 are the weights of flood susceptibility, flood depth, and rainfall,
 451 respectively. Although previous studies reported the efficacy of the classical AHP tool in
 452 modeling flood hazards (Pham et al. 2021a, Pham et al. 2021b), this study utilized a fuzzy
 453 AHP model (Zadeh 1996) due to its higher prediction accuracy (Büyükoğuzkan and Feyzioglu
 454 2004). First, fuzzy pairwise comparison matrices of the criteria and sub-criteria were
 455 developed using the triangular fuzzy numbers (TFN) of the scale of Saaty on relative
 456 importance (Ekmekcioğlu et al. 2021). Then weights of different criteria and the local
 457 weights of their sub-criteria were generated (Liou and Wang 1992). We also conducted a
 458 pairwise comparison of each alternative against every sub-criterion. Global weights of all
 459 sub-criterion were estimated by multiplying the weight of each criterion by their local
 460 weights. The flood susceptibility parameter was given the most importance, followed by
 461 rainfall and flood depth (Pham et al. 2021a). The higher values of all these three criteria
 462 indicate a higher flood hazard score. The validity of the weights was checked by ensuring a
 463 consistency ratio of less than 10%, where the consistency ratio is defined in equations (14)-
 464 (15) (Liou and Wang 1992).

$$Consistency\ Index = \frac{\lambda_{max} - k}{k - 1} \quad (14)$$

$$Consistency\ Ratio = \frac{Consistency\ Index}{Random\ Index} \quad (15)$$

466 where λ_{max} denotes the highest eigenvalue that belongs to the decision matrix and k
 467 is the number of criteria. We set a random index value consistent with the study of Saaty and
 468 Tran (2007). The optimism index was set to 80%. Finally, a weighted sum method was
 469 employed in equation (13) to estimate a flood hazard score.

470 *Flood exposure modeling*

471 The flood exposure score was estimated using equation (16) (Pham et al. 2021a, Pham et al.
 472 2021b).

$$Flood\ Exposure\ Score = A_2 \times Distance\ to\ River + B_2 \times LULC + C_2 \times Population\ Density \quad (16)$$

473 where A_2 , B_2 , and C_2 are the weights of distance to river, LULC, and population
 474 density, respectively. For designing fuzzy pairwise comparison matrices of criteria and sub-
 475 criteria for flood exposure modeling, the population density parameter was prioritized for its
 476 positive association with exposure (Pham et al. 2021b), followed by LULC and distance to
 477 river (Pham et al. 2021b).

478 *Flood vulnerability modeling*

479 The flood vulnerability score can be defined in equation (17) (Brito et al. 2018, Pham et al.
 480 2021a, Pham et al. 2021b).

$$Flood\ Vulnerability\ Score = A_3 \times Road\ Density + B_3 \times Age + C_3 \times Poverty\ (Wealth\ Index) \quad (17)$$

482 where A_3 , B_3 , and C_3 are the generated weights of road density, age, and poverty
 483 (wealth index) respectively utilizing the fuzzy AHP model. Here, poverty (wealth index) was
 484 given the highest preference (Pham et al. 2021a), followed by age and road density.

485
 486 *Flood risk modeling*

487 After estimating flood hazard, exposure, and vulnerability scores using fuzzy AHP models,
 488 we normalized their scores on a 0-1 scale. Finally, the flood risk map of Bangladesh was
 489 derived using equation (4) in GIS. In this study, all fuzzy AHP models were established using
 490 MATLAB R2020a software.

491 *Sensitivity analysis of flood causative factors*

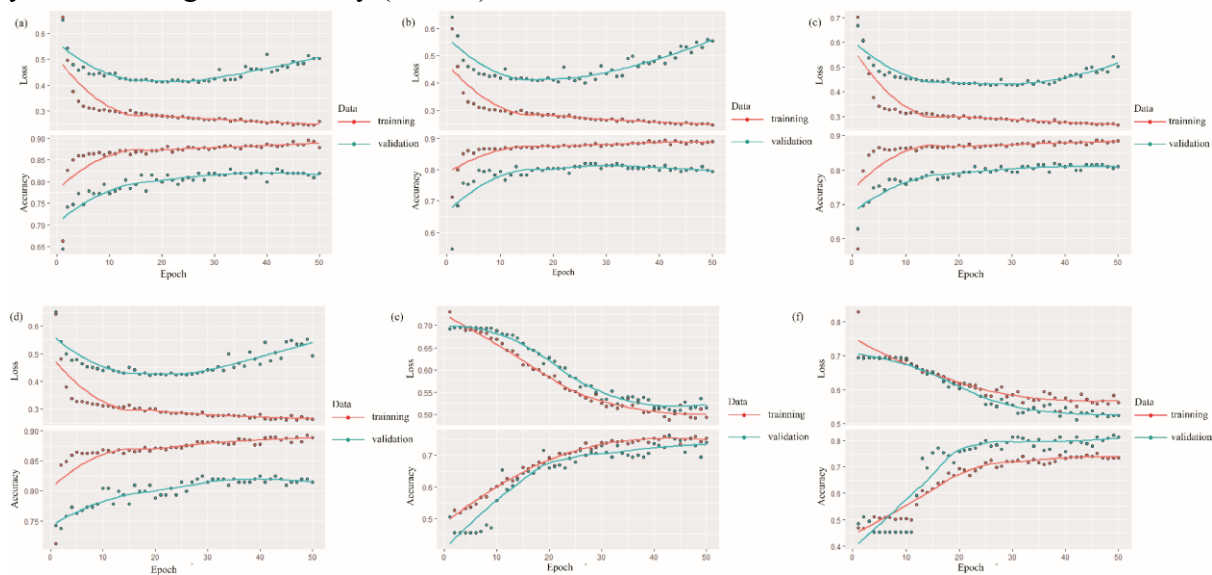
492 This study performed a sensitivity analysis of all the flood causative factors in modeling
 493 flood susceptibility, hazard, exposure, vulnerability, and risk by estimating their importance
 494 rank using the random forest (RF) function. The %IncMSE and IncNodePurity indicators
 495 were exploited to rank the flood causative factors, estimated using the ‘randomForest’
 496 package in R. The %IncMSE measures the upsurge in the MSE value of model prediction
 497 when the values of a feature are randomly permuted. The IncNodePurity indicates the total
 498 reduction of node impurities estimated by the Gini Index from variable splitting averaged
 499 over all the decision trees. The higher the values of %IncMSE and IncNodePurity suggest
 500 greater importance of a feature in the model — a greater sensitivity (Rahmati et al. 2020,
 501 Siam et al. 2021a).

502
 503 **Results**

504 *Flood susceptibility assessment*

505 *Standalone and hybridized DNN models*

506 Figure 4 shows the variation of the loss and accuracy metrics over the progression of 50
 507 epochs in each of the six DNN models on the train and validation datasets. The L2 – ADAM
 508 – ReLU – Softmax – DNN model is found to be the best-performed model for the train set,
 509 with an accuracy value of 0.8892. However, the ADAM – ReLU – Sigmoid – DNN model
 510 yielded the highest accuracy (0.8196) with validation data.



511

512 Figure 4. Variation of train loss and accuracy, validation loss and accuracy over the number
 513 of epochs for: (a) ADAM – ReLU – Sigmoid – DNN, (b) ADAM – ReLU – Softmax – DNN,
 514 (c) L2 – ADAM – ReLU – Sigmoid – DNN, (d) L2 – ADAM – ReLU – Softmax – DNN, (e)
 515 Dropout – ADAM – ReLU – Sigmoid – DNN and (f) Dropout – ADAM – ReLU – Softmax –
 516 DNN models.

517

518 *Standalone and hybridized SVR models*

519 In this study, the number of support vectors is found to be 1650, 1266, 1086, 1335, 756, and
 520 978 for standalone SVR, Gaussian RBF – SVR, GA – Gaussian RBF – SVR, GA – Laplacian
 521 RBF – SVR, GA – MLP – SVR, and GA – Linear – SVR models, respectively, during the
 522 training phase. This indicates that the MLP kernel reduces the complexity of the SVR model
 523 more compared to other kernels. The algorithm settings and solutions of GA – Gaussian RBF
 524 – SVR, GA – Laplacian RBF – SVR, GA – MLP – SVR, and GA – Linear – SVR are shown
 525 in Table 3.

526

527 Table 3. Settings and results of hybridized SVR models

Criteria		GA-Gaussian RBF-SVR	GA-Laplacian RBF-SVR	GA-MLP-SVR	GA-Linear-SVR	
GA Settings	Type	Real value	Real value	Real value	Real value	
	Population size	50	50	50	50	
	Number of generations	100	100	100	100	
	Elitism	2	2	2	2	
	Crossover probability	0.8	0.8	0.8	0.8	
	Mutation probability	0.1	0.1	0.1	0.1	
	Search domain	Epsilon	Lower	0	0	0
			Upper	1	1	1
	Gamma	Lower	0.0010	0.0010	-	-
		Upper	2.0000	2.0000	-	-
	Cost	Lower	0.0001	0.0001	0.0001	0.0001
		Upper	10	10	10	10
	Scale	Lower	-	-	0.00001	-
		Upper	-	-	1	-
Offset	Lower	-	-	-10	-	
	Upper	-	-	-0.00001	-	
GA Results	Iterations	100	100	100	100	
	Fitness function value	-0.0922	-0.0904	-0.1164	-0.1186	

Solution	Epsilon	0.1737	0.1020	0.6959	0.4982
	Gamma	0.1149	0.2989	-	-
	Cost	1.4114	9.3438	8.1556	5.1641
	Scale	-	-	0.1435	-
	Offset	-	-	-3.2567	-

528

529

530

531

532

533

534

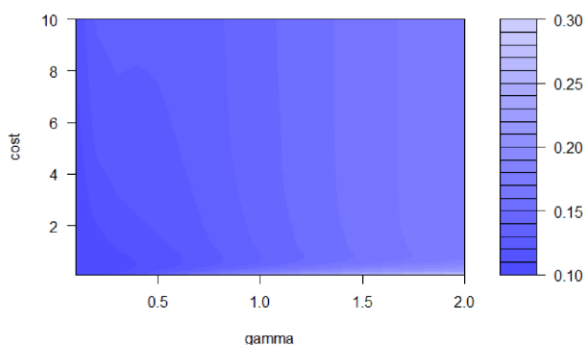
535

536

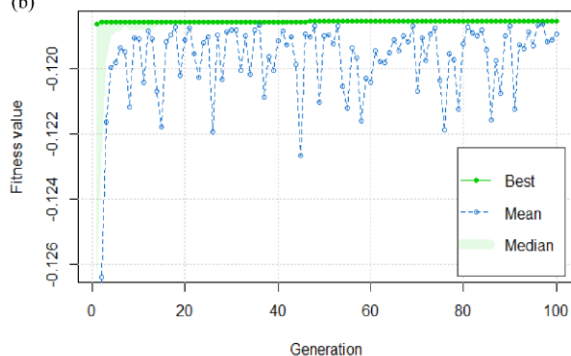
537

Figure 5 (a) shows the performance of all the trained Gaussian – RBF – SVR models using grid search in a contour plot where values of gamma are shown along the x-axis and values of cost are in the y-axis while the z-axis shows corresponding MSE. The optimal value of cost is 1.10 while the optimal gamma value is 0.10 for the best Gaussian RBF – SVR model with an MSE of 0.0925 from the grid search result. In the best Gaussian RBF – SVR model, weight values of slope, distance to river, drainage density, elevation, SPI, soil texture, soil permeability, LULC, geology, curvature, and aspect are -30.03, -40.58, 8.15, -47.18, 10.20, 18.70, 25.02, -2.52, 2.96, 0.09 and -0.08, respectively, where the bias is 0.39. The fitness values of the other four hybridized SVR models are shown in Figure 5 (b–e).

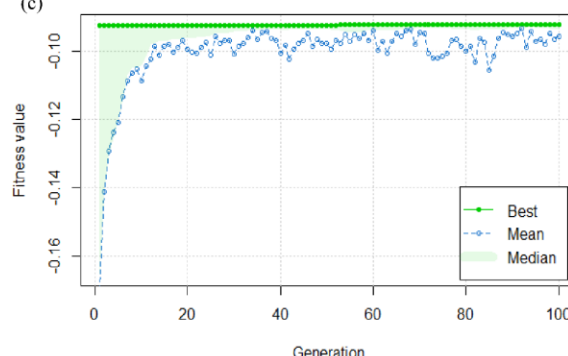
(a)



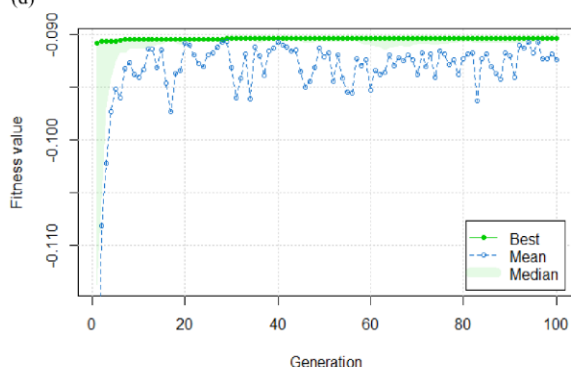
(b)



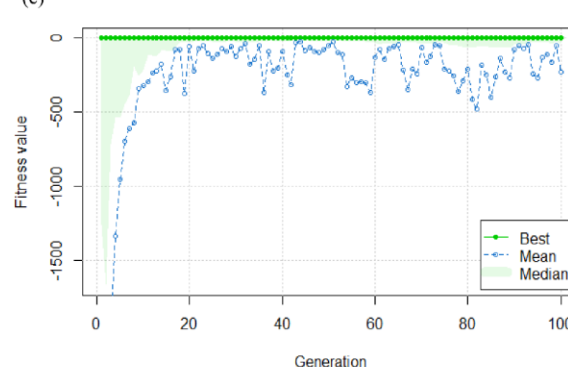
(c)



(d)



(e)

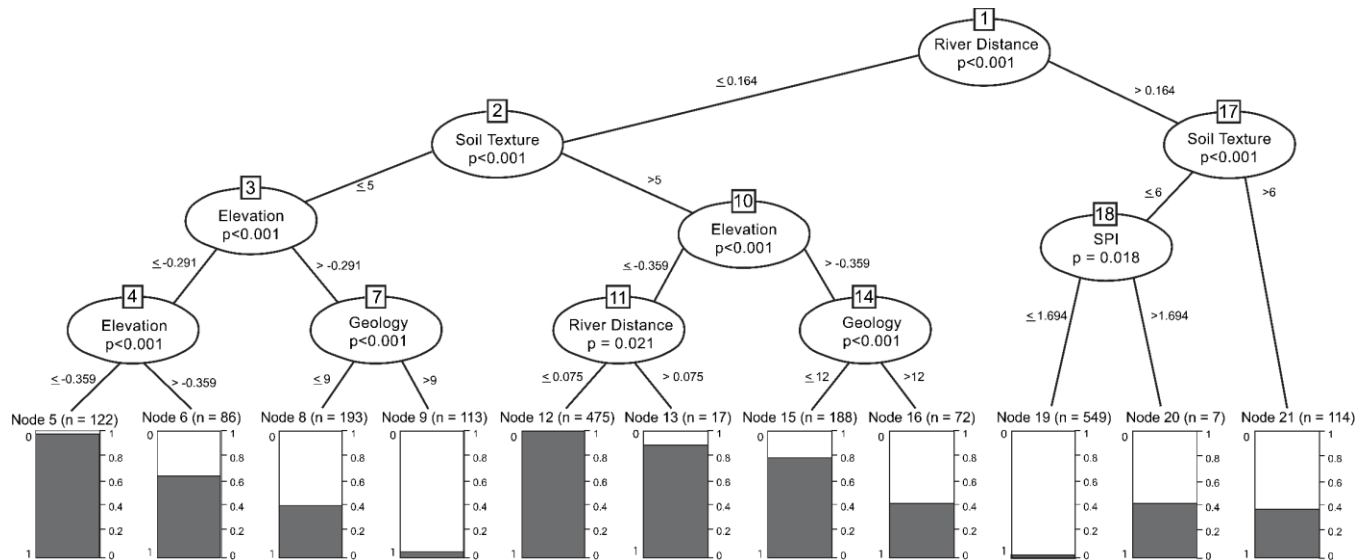


538

539 Figure 5. (a) Performance of all the trained Gaussian RBF – SVR models. Variation of fitness
 540 value over the number of generations in (b) GA – Linear – SVR, (c) GA – Gaussian RBF –
 541 SVR, (d) GA – Laplacian RBF – SVR and (e) GA – MLP – SVR models.
 542

543 *Conventional ML models*

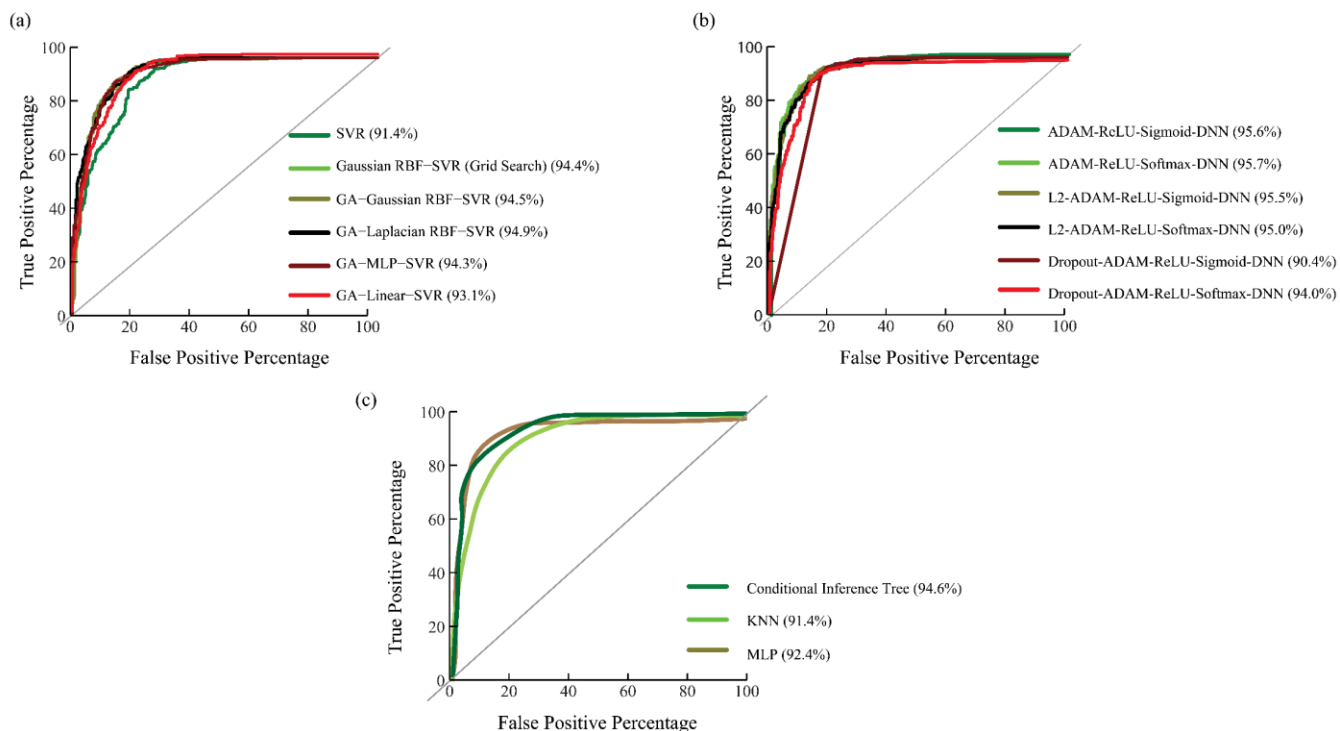
544 Among the other three ML models employed, the conditional inference tree performed better
 545 than KNN and MLP models in terms of fitting the train data more accurately. Figure 6
 546 illustrates the fitted conditional inference tree on the train set.



547
 548 Figure 6. Conditional inference tree based on train set

549
 550 *Model validation and comparison*

551 This study compares all fifteen ML models to select the best-performed model for flood
 552 susceptibility mapping in Bangladesh. Figure 7 illustrates the ROC curves of all models
 553 based on the test set.



554 Figure 7. Validation of (a) the standalone and hybridized SVR, (b) standalone and hybridized
 555 DNN and, (c) other machine learning models using the ROC curves
 556

557 The ADAM – ReLU – Softmax – DNN model yields the highest prediction accuracy,
 558 with an AUROC value of 95.7%, followed by the ADAM – ReLU – Sigmoid – DNN model
 559 (AUROC - 95.6%) and the L2 – ADAM – ReLU – Sigmoid – DNN model (AUROC -
 560 95.5%) (Figure 7 (b)). A total of four DNN models have an AUROC greater than or equal to
 561 95%. Contrarily, SVR models have relatively a lower prediction accuracy, where the GA –
 562 Laplacian RBF – SVR model obtained the highest AUROC value of 94.9% (Figure 7 (a)). In
 563 the case of conventional ML models, the conditional inference tree obtained the highest
 564 AUROC value of 94.6% (Figure 7 (c)). Model comparison results indicate a higher efficacy
 565 of the DNN models over the other models in estimating flood susceptibility. Table 4 presents
 566 the outcomes of performance assessment of different models.

567
 568 Table 4. Model performance using different statistical indices

Models	Cutoff	AUROC	OA	Kappa	Sensitivity	Specificity	PPV	NPV	MSE
ADAM-ReLU-Sigmoid-DNN	0.697	0.956	0.893	0.785	0.911	0.874	0.884	0.903	0.087
ADAM-ReLU-Softmax-DNN	0.507	0.957	0.894	0.788	0.929	0.857	0.872	0.920	0.083
L2- ADAM-ReLU-Sigmoid-DNN	0.603	0.955	0.898	0.795	0.927	0.867	0.880	0.919	0.084
L2- ADAM-ReLU-Softmax-DNN	0.848	0.950	0.883	0.766	0.894	0.872	0.880	0.887	0.108
Dropout- ADAM-ReLU-Sigmoid-DNN	0.618	0.904	0.887	0.773	0.960	0.810	0.841	0.951	0.117

Dropout- ADAM-ReLU- Softmax-DNN	0.429	0.940	0.892	0.783	0.941	0.840	0.860	0.932	0.140
SVR	0.554	0.914	0.847	0.693	0.878	0.815	0.833	0.864	0.126
Gaussian RBF-SVR	0.572	0.944	0.879	0.759	0.913	0.844	0.860	0.902	0.093
GA- Gaussian RBF-SVR	0.582	0.945	0.884	0.768	0.906	0.862	0.873	0.897	0.092
GA- Laplacian RBF-SVR	0.394	0.949	0.881	0.761	0.944	0.815	0.842	0.932	0.090
GA-MLP-SVR	0.525	0.943	0.883	0.766	0.908	0.857	0.869	0.899	0.116
GA-Linear -SVR	0.496	0.931	0.866	0.732	0.934	0.795	0.827	0.920	0.119
Conditional Inference Tree	0.639	0.946	0.869	0.740	0.812	0.931	0.925	0.825	0.087
KNN	0.600	0.914	0.842	0.684	0.873	0.810	0.828	0.859	0.114
MLP	0.633	0.924	0.879	0.759	0.915	0.842	0.859	0.905	0.108

569

570

571

572

573

574

575

576

577

578

579

580

581

582

583

584

585

586

587

588

589

590

591

592

593

594

595

596

597

The L2 – ADAM – ReLU – Sigmoid – DNN model obtains the highest OA value of 0.898 and a kappa statistic of 0.795, followed by the ADAM – ReLU – Softmax – DNN (OA = 0.894 and kappa = 0.788) and ADAM – ReLU – Sigmoid – DNN (OA = 0.893 and kappa = 0.785) models. However, the ADAM – ReLU – Softmax – DNN model achieves the lowest MSE value of 0.083, followed by the L2 – ADAM – ReLU – Sigmoid – DNN (MSE = 0.084) and ADAM – ReLU – Sigmoid – DNN (MSE = 0.087) models. Based on the AUROC, OA, kappa statistic, and MSE metrics together, this study identifies the L2 – ADAM – ReLU – Sigmoid – DNN and the ADAM-ReLU-Softmax-DNN models as the best two models for flood susceptibility mapping. However, the estimated SCAI values (Table 7) of flood susceptibility indicate that the hybridized L2 – ADAM – ReLU – Sigmoid – DNN model outperforms the ADAM-ReLU-Softmax-DNN model. Therefore, this study uses the hybridized L2 – ADAM – ReLU – Sigmoid – DNN model for mapping flood susceptibility in Bangladesh.

Flood hazard assessment

Figure 8 (b) shows the resultant flood hazard map. Among three criteria of flood hazard, flood susceptibility received the highest weight, followed by rainfall and flood depth (Table 5). About 20% of the total area is estimated to be flood hazard-prone zones of moderate to very high levels of severity. Southwestern and northeastern Bangladesh, as well as areas adjacent to major rivers, are high hazard zones (Figure 8 (b)). The SCAI of high and very high classes in the hazard map is the lowest, with values of 0.53 and 0.59, respectively (Table 6).

Flood exposure assessment

Figure 8 (c) shows the flood exposure map of Bangladesh. About 40% of the country is categorized as moderate to very high magnitudes. Among the three variables (distance to river, LULC, and population density), the estimated weight for population density is the highest (Table 5). Unsurprisingly, areas characterized by high population density are highly

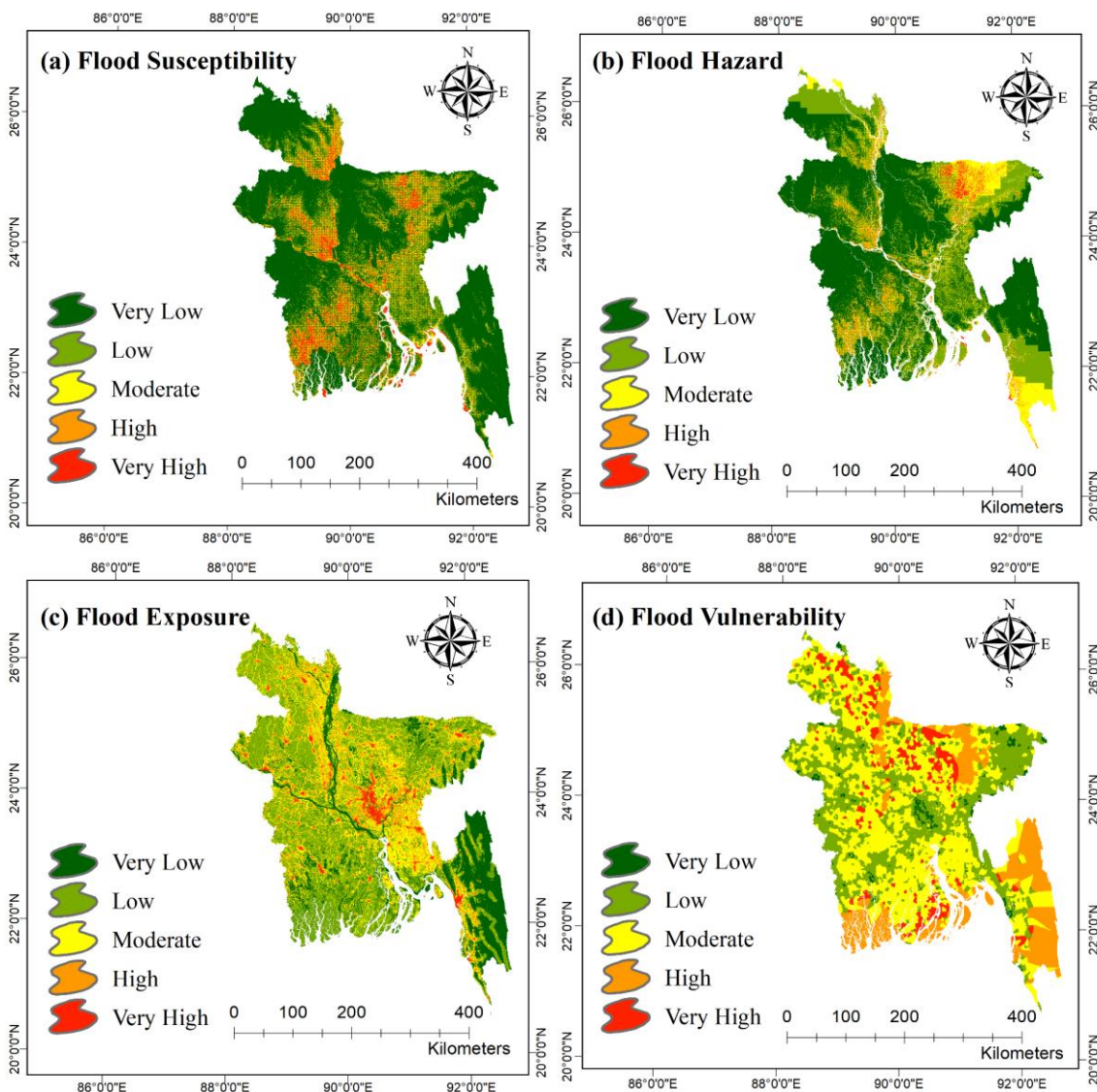
598 exposed to flooding.

599

600 **Flood vulnerability assessment**

601 The flood vulnerability map is shown in Figure 8 (d). Results show that about 69% of
 602 Bangladesh is vulnerable (moderate to very high) to flooding. The highest weight for the
 603 parameter wealth index (WI) (Table 5) indicates that the economic status of the people is one
 604 of the major determining flood vulnerability factors. Areas characterized by a low wealth
 605 index are highly vulnerable to flooding.

606



607

608 Figure 8. (a) Flood susceptibility, (b) flood hazard, (c) flood exposure and (d) flood
 609 vulnerability maps of Bangladesh

610

611 **Flood Risk Assessment**

612 Table 5 exhibits weights of criteria as well as sub-criteria for flood hazard, exposure, and
 613 vulnerability. Local weights indicate the type of association that exists between floods and
 614 various risk indicators. For instance, flood susceptibility, flood depth, rainfall, population

615 density, road density, and age are positively associated with flood risk. On the other hand,
 616 distance to river and wealth index are negatively correlated. In the case of LULC, built-up
 617 areas and croplands are highly prone to flood risk, particularly in areas with high flood
 618 potentials. In the case of the SCAI results, moderate to very high flood risk zones yield
 619 relatively low SCAI values. These results indicate a good agreement between the observed
 620 flood locations and modeled flood risk zones.

621

622

Table 5. Weights of criteria as well as sub-criteria generated by fuzzy AHP method

Component	Criteria	Weight	Class	Sub criteria	Local Weight	Global Weight
Flood Hazard	Flood susceptibility	0.6037	0 - 0.2	Very Low	0.0309	0.0187
			0.2 - 0.4	Low	0.0843	0.0509
			0.4 - 0.6	Moderate	0.1698	0.1025
			0.6 - 0.8	High	0.2870	0.1733
			0.8 - 1	Very High	0.4280	0.2584
	Flood depth	0.1003	No Flooding	1	0.0412	0.0041
			<0.30	2	0.0757	0.0076
			0.30 - 1.83	3	0.1223	0.0123
			1.83 - 3.05	4	0.2950	0.0296
			>3.05	5	0.4658	0.0467
	Rainfall	0.2960	245.4 - 333.7	1	0.0475	0.0141
			333.8 - 435.8	2	0.0870	0.0258
			435.9 - 560	3	0.1408	0.0417
			560.1 - 725.5	4	0.2770	0.0820
			725.6 – 949.02	5	0.4476	0.1325
Flood Exposure	Distance to river	0.0918	0 - 432	1	0.4199	0.0385
			432 - 1297	2	0.2597	0.0238
			1297 - 2594	3	0.1922	0.0176
			2594 - 4899	4	0.0937	0.0086
			4899 - 36890	5	0.0345	0.0032
LULC	0.3727	Water	1	0.0321	0.0120	
		Bare Land	2	0.0871	0.0325	
		Vegetation	3	0.2213	0.0825	
		Crops	4	0.2897	0.1080	
		Built Area	5	0.3698	0.1378	
Population density (Population per cell)	0.5355	0-1	1	0.0298	0.0160	
		1-2	2	0.1104	0.0591	
		2-3	3	0.1579	0.0846	
		3-6	4	0.2785	0.1491	
		6-370	5	0.4234	0.2267	
Flood Vulnerability	Road density	0.0859	0-0.9	1	0.0375	0.0032
			0.9 - 1.3	2	0.1046	0.0090
			1.3 - 1.6	3	0.1601	0.0138
			1.6 - 1.9	4	0.2287	0.0196
			1.9 - 3.4	5	0.4692	0.0403

Age (< 14 and > 60)	0.2643	0-1	1	0.0395	0.0104
		1-2	2	0.1110	0.0293
		2-3	3	0.1700	0.0449
		3-6	4	0.2433	0.0643
		6-101	5	0.4362	0.1153
Poverty (Wealth index)	0.6498	-1.2 - -0.61	1	0.4141	0.2691
		-0.6 - -0.3	2	0.2492	0.1619
		-0.29 - 0.07	3	0.1797	0.1168
		0.071 - 0.64	4	0.1237	0.0804
		0.65 - 2.2	5	0.0334	0.0217

623
624
625

Table 6: SCAI measurements of flood susceptibility, exposure, hazard, vulnerability and risk maps

Class	Flood Susceptibility (L2-ADAM-ReLU-Sigmoid-DNN)	Flood Susceptibility (ADAM-ReLU-Softmax-DNN)	Flood Exposure	Flood Hazard	Flood Vulnerability	Flood Risk
Very Low	1.56	3.24	1.56	1.49	1.20	1.40
Low	0.60	2.09	0.85	0.81	0.93	0.96
Moderate	0.63	1.92	0.97	0.66	0.91	0.66
High	0.53	1.89	0.97	0.53	1.55	0.59
Very High	0.56	0.68	3.17	0.59	1.04	0.67

626
627
628
629

Table 7 represents the consistency ratio for each component and criteria which is less than 10% i.e., acceptable in each case.

Table 7. Consistency ratio for flood risk components

Component	Consistency ratio (%)	Criteria	Consistency ratio (%)
Flood hazard	8.70	Flood susceptibility	9.88
		Flood depth	8.93

		Rainfall	6.17
Flood exposure	8.11	Distance to river	8.02
		LULC	7.79
		Population density	9.94
Flood vulnerability	4.19	Road density	7.61
		Age	5.88
		Poverty (Wealth index)	7.99

630

631

632

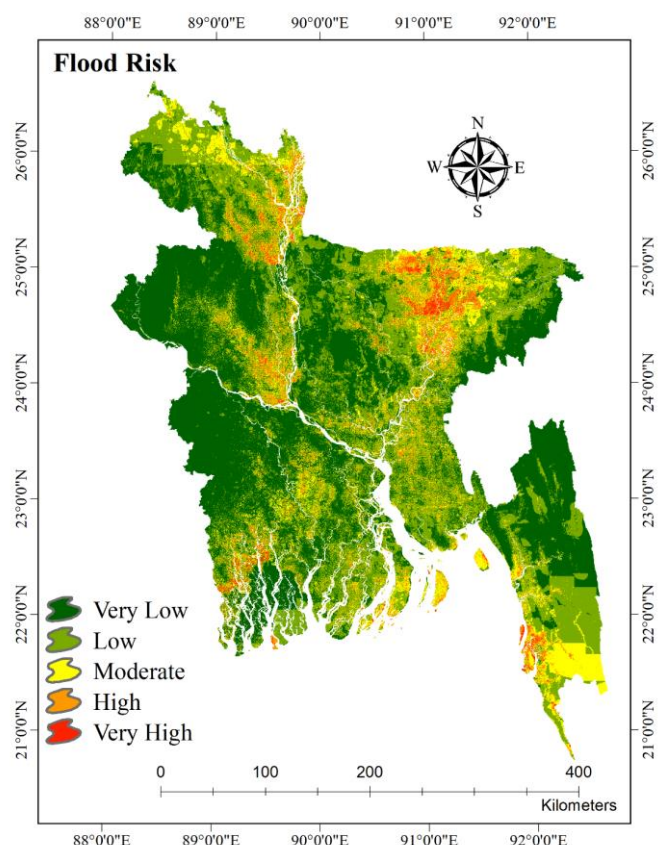
633

634

635

636

Figure 8 (a–d) illustrates the predicted flood susceptibility, flood hazard, flood exposure, and flood vulnerability maps of Bangladesh. The flood risk map obtained in this study is shown in Figure 9. About 20.45% of the area is categorized as flood risk zones, where the percentages of moderate, high, and very high flood risk-prone zones are 13.37%, 5.44%, and 1.64%, respectively. The northeastern region of Bangladesh, as well as areas near the GBM rivers, have high flood damage potential.



637

638

Figure 9. Flood risk map of Bangladesh

639

640

641

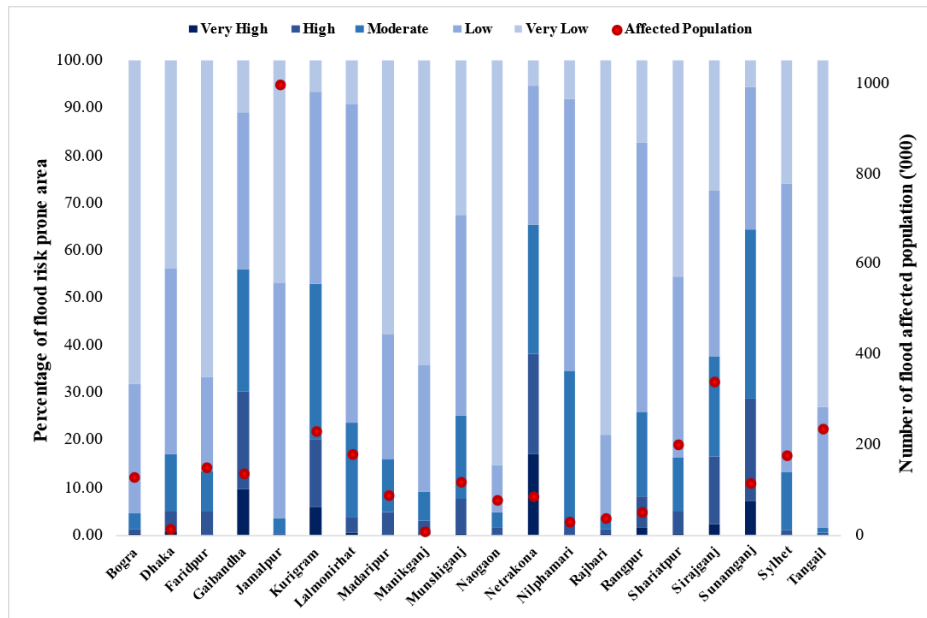
642

643

644

Figure 10 shows the percent of flood risk areas in a few districts where floods affected a significant number of people in 2020. For instance, in the Kurigram district, a total of 227,440 people (10.4% of the total population of Kurigram) were affected during monsoon flooding in 2020. This study found that about 52.95% of the total area of Kurigram district is a flood risk zone of moderate to very high severity. Similarly, in other northern districts such as Gaibandha, Nilphamari, and Ranpur, a significant number of people were flood-affected.

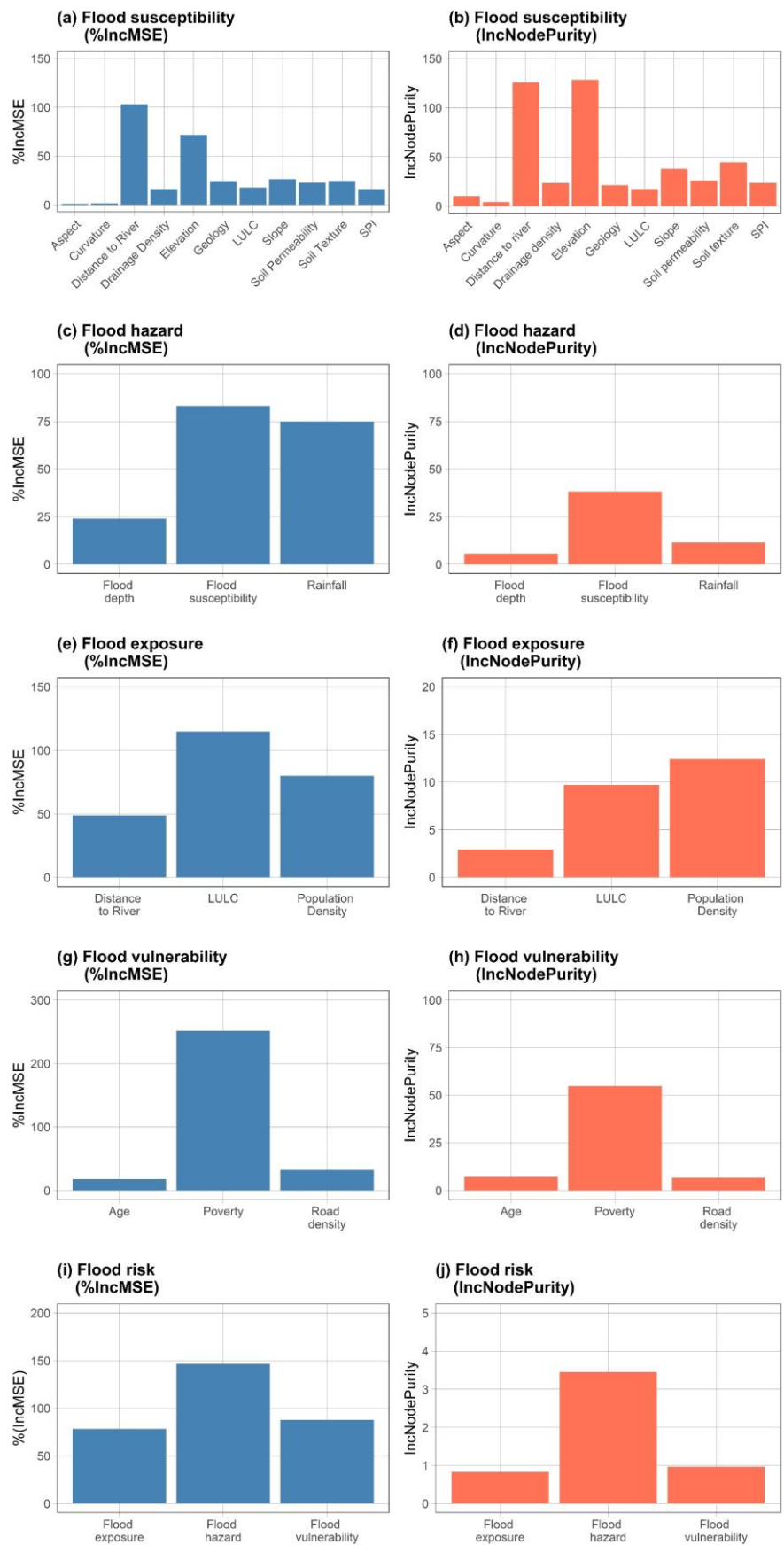
645 This study also found highly risk-prone regions. In the case of northeastern Bangladesh,
 646 districts such as Sunamganj and Netrakona are in this risk zone, with damage potential of
 647 64.43% and 65.38%, respectively. In these two districts, a total of 113,237 and 84,300 people
 648 were inflicted by floods in 2020 (CARE 2020).
 649



650
 651 Figure 10. Percentage of flood risk prone areas in different districts
 652

653 ***Sensitivity analysis results***

654 This study estimates the sensitivity of all corresponding factors in modeling flood
 655 susceptibility, hazard, exposure, vulnerability, and risk with respect to %IncMSE and
 656 IncNodePurity scores provided by RF. The flood susceptibility model is highly sensitive to
 657 factors such as elevation and distance to rivers (Figure 11 (a - b)). In the case of flood hazard,
 658 flood susceptibility is the most significant parameter (Figure 11(c - d)). LULC and population
 659 density are the important factors determining flood exposure (Figure 11(e - f)). In the case of
 660 flood vulnerability, poverty is the most influential factor (Figure 11(g - h)). Finally, this study
 661 notes that flood risk is sensitive to flood hazard (Figure 11(i - j)). A recent study (Adnan et al.
 662 2020a) validates the results of flood exposure, vulnerability, and risk.
 663



664
665
666

Figure 11. Sensitivity analysis of flood causative factors in modeling flood susceptibility, hazard, exposure, vulnerability and risk based on %IncMSE and IncNodePurity.

667 Discussion

668 This study aimed to present a flood risk assessment framework using hybridized DNN and
 669 fuzzy AHP models, hypothesizing that the use of hybridized models would improve the
 670 accuracy of flood risk models. Hence, we developed and evaluated the performance of fifteen
 671 models including twelve standalone and hybridized ML models and three conventional ML
 672 models. The results exhibit the efficacy of the hybridized DNN architectures over all other
 673 models. This is a first attempt to combine hybridized DNN architectures with fuzzy AHP
 674 models to assess flood risk in a complex flood regime like deltaic Bangladesh.

675 In the case of flood susceptibility, elevation and distance to river were found as the
 676 most influential factors influencing flood potentials. Both these findings are supported by
 677 other recent studies (Wang et al. 2019, Rahmati et al. 2020, Chou et al. 2021, Pham et al.
 678 2021a, Pham et al. 2021b). This study established a total of fifteen flood susceptibility
 679 models that produced an AUC value of more than 90%, indicating an excellent prediction
 680 accuracy (Arabameri et al. 2019). Flood susceptibility map produced using the hybridized L2
 681 – ADAM – ReLU – Sigmoid – DNN model (Figure 8 (a)) yielded the highest prediction
 682 accuracy, resulting in a good agreement with the flood inundation map of Bangladesh in
 683 2020.

684 The flood susceptibility map produced in this study showed that the northeastern part of
 685 Bangladesh is highly susceptible, including Netrokona, Sunamganj, Kishoreganj, and
 686 Mymensingh. These districts are also in high-risk-prone zones. All these districts include large
 687 water bodies (locally known as “*Haor*”) and faced severe flooding in the last couple of years.
 688 These districts are also characterized by a low slope and elevation. A recent study reported that
 689 areas with a lower slope and elevation have greater flood damage potential (Adnan et al.
 690 2020b). On the contrary, districts in the southeastern zone such as Khagrachori and Banderbans
 691 are characterized by high elevation areas and low-density population; hence, pose a relatively
 692 low risk. These districts mostly remained inundation-free during the flood events of 2020
 693 (Figure 2). This finding is in accord with other studies that noted that elevation has an inverse
 694 relationship with flooding in general (Rahman et al. 2021b). The flood risk map produced in
 695 this study showed that several districts in northern and northeastern parts of Bangladesh are
 696 located in a high-risk zone, where a significant number of people were affected during the 2020
 697 flood event. Previous studies also reported that the flood potentials of these districts are very
 698 high primarily due to their proximity to major rivers (Rahman et al. 2019, Siam et al. 2021a).
 699 This finding is also consistent with studies that mentioned that areas closer to the rivers are
 700 highly at risk of flood disaster (Talukdar et al. 2020). This study also noted that flood hazard,
 701 vulnerability, and risk models are sensitive to flood susceptibility, poverty, and flood hazard,
 702 respectively. Several recent studies (Adnan et al. 2020a, Adnan et al. 2020b, Siam et al. 2021a)
 703 validates the results of flood hazard, vulnerability, and risk.

704 Although the proposed framework resulted in a very high flood risk prediction
 705 accuracy, several limitations and uncertainties can be anticipated. First, this study considered
 706 only one flood event due to the unavailability of long-term flood observation data at the
 707 national level. Second, flood susceptibility, hazard, exposure, and vulnerability indicators’
 708 data had differing spatial resolutions. For these reasons, the independent and dependent
 709 variables used in this study might be subject to label noise. A recent study has observed

710 negative effects of label noise on the performance of ML-based flood susceptibility modeling
 711 (Siam et al. 2021b). Future research can address these limitations by establishing label noise-
 712 tolerant standalone and hybridized ML models.

713

714 **Conclusion**

715 In the present study, a novel approach to flood risk assessment in Bangladesh was developed,
 716 combining hybridized DNN and fuzzy AHP methods. Based on various model performance
 717 assessment indices, the hybridized L2 – ADAM – ReLU – Sigmoid – DNN model was
 718 selected as the best-performed flood susceptibility model. The resultant flood susceptibility
 719 map was used to develop a flood hazard map utilizing the fuzzy AHP model. Finally, the
 720 flood risk map of Bangladesh was developed by integrating flood hazard, exposure, and
 721 vulnerability maps. Despite some uncertainties and limitations, the study promotes the use of
 722 hybridized DNN model for spatial flood risk modeling to achieve a country-scale flood risk
 723 map. The proposed flood risk assessment framework is expected to be useful for
 724 policymakers to better manage flood risk. For future research, this study can be extended to
 725 appraise spatiotemporal flood risk assessment using hybridized DNN models.

726

727 **Acknowledgements**

728 This work is supported by the ICT Innovation Fund (2020-21) provided by the ICT division, Ministry
 729 of Post, Telecommunication and Information Technology of the People’s Republic of Bangladesh.

730

731 **Data and code availability statement**

732 The data and codes that support the findings of this study are available from the
 733 corresponding author upon reasonable request.

734

735 **References**

- 736 Adnan, M.S.G., Abdullah, A.Y.M., Dewan, A. & Hall, J.W., 2020a. The effects of changing
 737 land use and flood hazard on poverty in coastal bangladesh. *Land Use Policy*, 99,
 738 104868.
- 739 Adnan, M.S.G., Dewan, A., Zannat, K.E. & Abdullah, A.Y.M., 2019a. The use of watershed
 740 geomorphic data in flash flood susceptibility zoning: A case study of the karnaphuli
 741 and sangu river basins of bangladesh. *Natural Hazards*, 99 (1), 425-448.
- 742 Adnan, M.S.G., Haque, A. & Hall, J.W., 2019b. Have coastal embankments reduced flooding
 743 in bangladesh? *Science of the total environment*, 682, 405-416.
- 744 Adnan, M.S.G., Talchabhadel, R., Nakagawa, H. & Hall, J.W., 2020b. The potential of tidal
 745 river management for flood alleviation in south western bangladesh. *Science of The*
 746 *Total Environment*, 731, 138747 %@ 0048-9697.
- 747 Ahmadi, M., Al-Fugara, A.K., Al-Shabeeb, A.R., Arora, A., Al-Adamat, R., Pham, Q.B.,
 748 Al-Ansari, N., Linh, N.T.T. & Sajedi, H., 2021. Flood susceptibility mapping and
 749 assessment using a novel deep learning model combining multilayer perceptron and
 750 autoencoder neural networks. *Journal of Flood Risk Management*, 14 (1), e12683.
- 751 Akay, H., 2021. Flood hazards susceptibility mapping using statistical, fuzzy logic, and mcdm
 752 methods. *Soft Computing*, 25 (14), 9325-9346.
- 753 Akay, H. & Baduna Koçyiğit, M., 2020. Flash flood potential prioritization of sub-basins in an
 754 ungauged basin in turkey using traditional multi-criteria decision-making methods. *Soft*
 755 *Computing*, 24 (18), 14251-14263.

- 756 Arabameri, A., Rezaei, K., Cerdà, A., Conoscenti, C. & Kalantari, Z., 2019. A comparison of
 757 statistical methods and multi-criteria decision making to map flood hazard
 758 susceptibility in northern Iran. *Science of the Total Environment*, 660, 443-458.
- 759 Bai, S., Lü, G., Wang, J., Zhou, P. & Ding, L., 2011. Gis-based rare events logistic regression
 760 for landslide-susceptibility mapping of lianyungang, China. *Environmental Earth
 761 Sciences*, 62 (1), 139-149.
- 762 Bannari, A., Ghadeer, A., El-Battay, A., Hameed, N. & Rouai, M., 2017. Detection of areas
 763 associated with flash floods and erosion caused by rainfall storm using topographic
 764 attributes, hydrologic indices, and GIS. *Global changes and natural disaster
 765 management: Geo-information technologies*. Springer, 155-174.
- 766 Barbour, E.J., Adnan, M.S.G., Borgomeo, E., Paprocki, K., Khan, S.A., Salehin, M. & Hall,
 767 J.W., 2022. The unequal distribution of water risks and adaptation benefits in coastal
 768 Bangladesh. *Nature Sustainability*.
- 769 Barc, 2014. Land resource database. In (Barc), B.a.R.C. ed. Dhaka, Bangladesh
- 770 Bondarenko, M., Kerr, D., Sorichetta, A. & Tatem, A.J., 2020. Estimates of 2020 total number
 771 of people per grid square, adjusted to match the corresponding unpd 2020 estimates and
 772 broken down by gender and age groupings, produced using built-settlement growth
 773 model (bsgm) outputs. UK: University of Southampton.
- 774 Brito, M.M.D., Evers, M. & Almoradie, A.D.S., 2018. Participatory flood vulnerability
 775 assessment: A multi-criteria approach. *Hydrology and Earth System Sciences*, 22 (1),
 776 373-390.
- 777 Bui, D.T., Hoang, N.-D., Martínez-Álvarez, F., Ngo, P.-T.T., Hoa, P.V., Pham, T.D., Samui,
 778 P. & Costache, R., 2020a. A novel deep learning neural network approach for predicting
 779 flash flood susceptibility: A case study at a high frequency tropical storm area. *Science
 780 of The Total Environment*, 701, 134413.
- 781 Bui, D.T., Ngo, P.-T.T., Pham, T.D., Jaafari, A., Minh, N.Q., Hoa, P.V. & Samui, P., 2019. A
 782 novel hybrid approach based on a swarm intelligence optimized extreme learning
 783 machine for flash flood susceptibility mapping. *Catena*, 179, 184-196.
- 784 Bui, Q.-T., Nguyen, Q.-H., Nguyen, X.L., Pham, V.D., Nguyen, H.D. & Pham, V.-M., 2020b.
 785 Verification of novel integrations of swarm intelligence algorithms into deep learning
 786 neural network for flood susceptibility mapping. *Journal of Hydrology*, 581, 124379.
- 787 Büyükköçkan, G. & Feyzioğlu, O., 2004. A fuzzy-logic-based decision-making approach for
 788 new product development. *International journal of production economics*, 90 (1), 27-
 789 45.
- 790 Care, 2020. *Monsoon floods 2020 - coordinated preliminary impact and needs assessment*.
- 791 Chen, J., Huang, G. & Chen, W., 2021. Towards better flood risk management: Assessing flood
 792 risk and investigating the potential mechanism based on machine learning models.
 793 *Journal of environmental management*, 293, 112810.
- 794 Chou, T.Y., Hoang, T.V., Fang, Y.M., Nguyen, Q.H., Lai, T.A., Pham, V.M., Vu, V.M. & Bui,
 795 Q.T., 2021. Swarm-based optimizer for convolutional neural network: An application
 796 for flood susceptibility mapping. *Transactions in GIS*, 25 (2), 1009-1026.
- 797 Chowdhury, E.H. & Hassan, Q.K., 2017. Use of remote sensing data in comprehending an
 798 extremely unusual flooding event over southwest Bangladesh. *Natural Hazards*, 88 (3),
 799 1805-1823.
- 800 Costache, R., Ali, S.A., Parvin, F., Pham, Q.B., Arabameri, A., Nguyen, H., Crăciun, A. &
 801 Anh, D.T., 2021. Detection of areas prone to flood-induced landslides risk using
 802 certainty factor and its hybridization with fahp, xgboost and deep learning neural
 803 network. *Geocarto International*, 1-36.
- 804 Costache, R., Pham, Q.B., Sharifi, E., Linh, N.T.T., Abba, S.I., Vojtek, M., Vojteková, J., Nhi,
 805 P.T.T. & Khoi, D.N., 2020a. Flash-flood susceptibility assessment using multi-criteria

- 806 decision making and machine learning supported by remote sensing and gis techniques.
 807 *Remote Sensing*, 12 (1), 106.
- 808 Costache, R., Popa, M.C., Bui, D.T., Diaconu, D.C., Ciubotaru, N., Minea, G. & Pham, Q.B.,
 809 2020b. Spatial predicting of flood potential areas using novel hybridizations of fuzzy
 810 decision-making, bivariate statistics, and machine learning. *Journal of Hydrology*, 585,
 811 124808.
- 812 Darabi, H., Choubin, B., Rahmati, O., Haghighi, A.T., Pradhan, B. & Kløve, B., 2019. Urban
 813 flood risk mapping using the garp and quest models: A comparative study of machine
 814 learning techniques. *Journal of hydrology*, 569, 142-154.
- 815 David, A. & Schmalz, B., 2020. Flood hazard analysis in small catchments: Comparison of
 816 hydrological and hydrodynamic approaches by the use of direct rainfall. *Journal of*
 817 *Flood Risk Management*, 13 (4), e12639.
- 818 De Moel, H., Jongman, B., Kreibich, H., Merz, B., Penning-Rowsell, E. & Ward, P.J., 2015.
 819 Flood risk assessments at different spatial scales. *Mitigation and Adaptation Strategies*
 820 *for Global Change*, 20 (6), 865-890.
- 821 Dewan, A.M. & Kankam-Yeboah, K., 2006. Using synthetic aperture radar (sar) data for
 822 mapping river water flooding in an urban landscape: A case study of greater dhaka,
 823 bangladesh. *Journal of Japan Society of Hydrology and Water Resources*, 19 (1), 44-
 824 54.
- 825 Dewan, T.H., 2015. Societal impacts and vulnerability to floods in bangladesh and nepal.
 826 *Weather and Climate Extremes*, 7, 36-42.
- 827 Ekmekcioğlu, Ö., Koc, K. & Özger, M., 2021. District based flood risk assessment in istanbul
 828 using fuzzy analytical hierarchy process. *Stochastic Environmental Research and Risk*
 829 *Assessment*, 35 (3), 617-637.
- 830 Hasan, S.S., Deng, X., Li, Z. & Chen, D., 2017. Projections of future land use in bangladesh
 831 under the background of baseline, ecological protection and economic development.
 832 *Sustainability*, 9 (4), 505.
- 833 Huffman, G.J., Stocker, E.F., Bolvin, D.T., Nelkin, E.J. & Tan, J., 2019. Gpm imerg final
 834 precipitation l3 half hourly 0.1 degree x 0.1 degree v06, greenbelt, md, goddard earth
 835 sciences data and information services center (ges disc). The National Aeronautics and
 836 Space Administration (NASA).
- 837 Islam, A.R.M.T., Talukdar, S., Mahato, S., Kundu, S., Eibek, K.U., Pham, Q.B., Kuriqi, A. &
 838 Linh, N.T.T., 2021. Flood susceptibility modelling using advanced ensemble machine
 839 learning models. *Geoscience Frontiers*, 12 (3), 101075.
- 840 Islam, M.M. & Sado, K., 2000. Flood hazard assessment in bangladesh using noaa avhrr data
 841 with geographical information system. *Hydrological Processes*, 14 (3), 605-620.
- 842 Jaxa, 2015. Alos global digital surface model “alos world 3d-30m (aw3d30)”.
- 843 Karra, K., Kontgis, C., Statman-Weil, Z., Mazzariello, J., Mathis, M. & Brumby, S., Year.
 844 Global land use / land cover with sentinel 2 and deep learning. eds. *IGARSS 2021-*
 845 *2021 IEEE International Geoscience and Remote Sensing Symposium*, United States:
 846 IEEE.
- 847 Leon, M.A., Barua, P., Sarker, P., Kumar, P. & Hasan, M., 2020. *Annual flood report 2019*.
- 848 Liou, T.-S. & Wang, M.-J.J., 1992. Ranking fuzzy numbers with integral value. *Fuzzy sets and*
 849 *systems*, 50 (3), 247-255.
- 850 Lu, Y., Bookman, R., Waldmann, N. & Marco, S., 2020. A 45 kyr laminae record from the
 851 dead sea: Implications for basin erosion and floods recurrence. *Quaternary Science*
 852 *Reviews*, 229, 106143.
- 853 Luu, C., Von Meding, J. & Mojtahedi, M., 2019. Analyzing vietnam's national disaster loss
 854 database for flood risk assessment using multiple linear regression-topsis. *International*
 855 *Journal of Disaster Risk Reduction*, 40, 101153.

- 856 Ma, L., Liu, Y., Zhang, X., Ye, Y., Yin, G. & Johnson, B.A., 2019a. Deep learning in remote
857 sensing applications: A meta-analysis and review. *ISPRS journal of photogrammetry*
858 *and remote sensing*, 152, 166-177.
- 859 Ma, M., Liu, C., Zhao, G., Xie, H., Jia, P., Wang, D., Wang, H. & Hong, Y., 2019b. Flash flood
860 risk analysis based on machine learning techniques in the yunnan province, china.
861 *Remote Sensing*, 11 (2), 170.
- 862 Meyer, V., Scheuer, S. & Haase, D., 2009. A multicriteria approach for flood risk mapping
863 exemplified at the mulde river, germany. *Natural hazards*, 48 (1), 17-39.
- 864 Midi, H., Sarkar, S.K. & Rana, S., 2010. Collinearity diagnostics of binary logistic regression
865 model. *Journal of Interdisciplinary Mathematics*, 13 (3), 253-267.
- 866 Mojaddadi, H., Pradhan, B., Nampak, H., Ahmad, N. & Ghazali, A.H.B., 2017. Ensemble
867 machine-learning-based geospatial approach for flood risk assessment using multi-
868 sensor remote-sensing data and gis. *Geomatics, Natural Hazards and Risk*, 8 (2), 1080-
869 1102.
- 870 Nasa, 2020. Intense flooding in bangladesh. The National Aeronautics and Space
871 Administration (NASA).
- 872 Ngo, P.-T.T., Pham, T.D., Hoang, N.-D., Tran, D.A., Amiri, M., Le, T.T., Hoa, P.V., Van Bui,
873 P., Nhu, V.-H. & Bui, D.T., 2021. A new hybrid equilibrium optimized sysfor based
874 geospatial data mining for tropical storm-induced flash flood susceptible mapping.
875 *Journal of Environmental Management*, 280, 111858.
- 876 Nguyen, H.D., Nguyen, Q.-H., Du, Q.V.V., Nguyen, T.H.T., Nguyen, T.G. & Bui, Q.-T., 2021.
877 A novel combination of deep neural network and manta ray foraging optimization for
878 flood susceptibility mapping in quang ngai province, vietnam. *Geocarto International*,
879 1-25.
- 880 Panahi, M., Jaafari, A., Shirzadi, A., Shahabi, H., Rahmati, O., Omidvar, E., Lee, S. & Bui,
881 D.T., 2021. Deep learning neural networks for spatially explicit prediction of flash
882 flood probability. *Geoscience Frontiers*, 12 (3), 101076.
- 883 Pappenberger, F., Matgen, P., Beven, K.J., Henry, J.-B. & Pfister, L., 2006. Influence of
884 uncertain boundary conditions and model structure on flood inundation predictions.
885 *Advances in water resources*, 29 (10), 1430-1449.
- 886 Paul, G.C., Saha, S. & Hembram, T.K., 2019. Application of the gis-based probabilistic models
887 for mapping the flood susceptibility in bansloi sub-basin of ganga-bhagirathi river and
888 their comparison. *Remote Sensing in Earth Systems Sciences*, 2 (2), 120-146.
- 889 Persits, F.M., Wandrey, C.J., Milici, R.C. & Manwar, A., 2001. Digital geologic and
890 geophysical data of bangladesh: U.S. Geological survey open-file report 97-470-h. U.S.
891 Geological Survey.
- 892 Pham, B.T., Luu, C., Van Dao, D., Van Phong, T., Nguyen, H.D., Van Le, H., Von Meding, J.
893 & Prakash, I., 2021a. Flood risk assessment using deep learning integrated with multi-
894 criteria decision analysis. *Knowledge-Based Systems*, 219, 106899.
- 895 Pham, B.T., Luu, C., Van Phong, T., Nguyen, H.D., Van Le, H., Tran, T.Q., Ta, H.T. &
896 Prakash, I., 2021b. Flood risk assessment using hybrid artificial intelligence models
897 integrated with multi-criteria decision analysis in quang nam province, vietnam.
898 *Journal of Hydrology*, 592, 125815.
- 899 Planchon, O. & Darboux, F., 2002. A fast, simple and versatile algorithm to fill the depressions
900 of digital elevation models. *Catena*, 46 (2-3), 159-176.
- 901 Pradhan, B., 2010. Flood susceptible mapping and risk area delineation using logistic
902 regression, gis and remote sensing. *Journal of Spatial Hydrology*, 9 (2).
- 903 Rahman, M., Chen, N., Elbeltagi, A., Islam, M.M., Alam, M., Pourghasemi, H.R., Tao, W.,
904 Zhang, J., Shufeng, T. & Faiz, H., 2021a. Application of stacking hybrid machine

- 905 learning algorithms in delineating multi-type flooding in bangladesh. *Journal of*
 906 *Environmental Management*, 295, 113086.
- 907 Rahman, M., Ningsheng, C., Islam, M.M., Dewan, A., Iqbal, J., Washakh, R.M.A. & Shufeng,
 908 T., 2019. Flood susceptibility assessment in bangladesh using machine learning and
 909 multi-criteria decision analysis. *Earth Systems and Environment*, 3 (3), 585-601.
- 910 Rahman, M., Ningsheng, C., Mahmud, G.I., Islam, M.M., Pourghasemi, H.R., Ahmad, H.,
 911 Habumugisha, J.M., Washakh, R.M.A., Alam, M. & Liu, E., 2021b. Flooding and its
 912 relationship with land cover change, population growth, and road density. *Geoscience*
 913 *Frontiers*, 12 (6), 101224.
- 914 Rahmati, O., Darabi, H., Panahi, M., Kalantari, Z., Naghibi, S.A., Ferreira, C.S.S., Kornejady,
 915 A., Karimidastenaei, Z., Mohammadi, F. & Stefanidis, S., 2020. Development of novel
 916 hybridized models for urban flood susceptibility mapping. *Scientific Reports*, 10 (1), 1-
 917 19.
- 918 Rincón, D., Khan, U.T. & Armenakis, C., 2018. Flood risk mapping using gis and multi-criteria
 919 analysis: A greater toronto area case study. *Geosciences*, 8 (8), 275 Available from:
 920 <https://www.mdpi.com/2076-3263/8/8/275>.
- 921 Ronco, P., Bullo, M., Torresan, S., Critto, A., Olschewski, R., Zappa, M. & Marcomini, A.,
 922 2015. Kulturisk regional risk assessment methodology for water-related natural
 923 hazards–part 2: Application to the zurich case study. *Hydrology and Earth System*
 924 *Sciences*, 19 (3), 1561-1576.
- 925 Saaty, T.L. & Tran, L.T., 2007. On the invalidity of fuzzifying numerical judgments in the
 926 analytic hierarchy process. *Mathematical and Computer Modelling*, 46 (7-8), 962-975.
- 927 Sarkar, D. & Mondal, P., 2020. Flood vulnerability mapping using frequency ratio (fr) model:
 928 A case study on kulik river basin, indo-bangladesh barind region. *Applied Water*
 929 *Science*, 10 (1), 1-13.
- 930 Siam, Z.S., Hasan, R.T., Anik, S.S., Noor, F., Adnan, M.S.G. & Rahman, R.M., Year. Study
 931 of hybridized support vector regression based flood susceptibility mapping for
 932 bangladesh. ^eds. *International Conference on Industrial, Engineering and Other*
 933 *Applications of Applied Intelligent Systems* Springer, 59-71.
- 934 Siam, Z.S., Hasan, R.T. & Rahman, R.M., 2021b. Effects of label noise on regression
 935 performances and model complexities for hybridized machine learning based spatial
 936 flood susceptibility modelling. *Cybernetics and Systems*, 1-18.
- 937 Singh, V.K., Kumar, D., Kashyap, P., Singh, P.K., Kumar, A. & Singh, S.K., 2020. Modelling
 938 of soil permeability using different data driven algorithms based on physical properties
 939 of soil. *Journal of Hydrology*, 580, 124223.
- 940 Steele, J.E., Sundsøy, P.R., Pezzulo, C., Alegana, V.A., Bird, T.J., Blumenstock, J., Bjelland,
 941 J., Engø-Monsen, K., De Montjoye, Y.-A. & Iqbal, A.M., 2017. Mapping poverty using
 942 mobile phone and satellite data. *Journal of The Royal Society Interface*, 14 (127),
 943 20160690.
- 944 Stefanidis, S. & Stathis, D., 2013. Assessment of flood hazard based on natural and
 945 anthropogenic factors using analytic hierarchy process (ahp). *Natural hazards*, 68 (2),
 946 569-585.
- 947 Talukdar, S., Ghose, B., Salam, R., Mahato, S., Pham, Q.B., Linh, N.T.T., Costache, R. &
 948 Avand, M., 2020. Flood susceptibility modeling in teesta river basin, bangladesh using
 949 novel ensembles of bagging algorithms. *Stochastic Environmental Research and Risk*
 950 *Assessment*, 34 (12), 2277-2300.
- 951 Tehrany, M.S., Pradhan, B., Mansor, S. & Ahmad, N., 2015. Flood susceptibility assessment
 952 using gis-based support vector machine model with different kernel types. *Catena*, 125,
 953 91-101.

- 954 Tehrany, M.S., Shabani, F., Neamah Jebur, M., Hong, H., Chen, W. & Xie, X., 2017. Gis-
 955 based spatial prediction of flood prone areas using standalone frequency ratio, logistic
 956 regression, weight of evidence and their ensemble techniques. *Geomatics, Natural*
 957 *Hazards and Risk*, 8 (2), 1538-1561.
- 958 Thirumurugan, P. & Krishnaveni, M., 2019. Flood hazard mapping using geospatial techniques
 959 and satellite images—a case study of coastal district of tamil nadu. *Environmental*
 960 *monitoring and assessment*, 191 (3), 1-17.
- 961 Unitar, 2020. Satellite detected water extent in bangladesh. Geneva, Switzerland: United
 962 Nations Institute for Training and Research (UNITAR)
- 963 Vilasan, R. & Kapse, V.S., 2021. Evaluation of the prediction capability of ahp and f_ahp
 964 methods in flood susceptibility mapping of ernakulam district (india).
- 965 Wang, Y., Fang, Z., Hong, H. & Peng, L., 2020. Flood susceptibility mapping using
 966 convolutional neural network frameworks. *Journal of Hydrology*, 582, 124482.
- 967 Wang, Y., Hong, H., Chen, W., Li, S., Panahi, M., Khosravi, K., Shirzadi, A., Shahabi, H.,
 968 Panahi, S. & Costache, R., 2019. Flood susceptibility mapping in dingnan county
 969 (china) using adaptive neuro-fuzzy inference system with biogeography based
 970 optimization and imperialistic competitive algorithm. *Journal of environmental*
 971 *management*, 247, 712-729.
- 972 Wang, Y., Li, Z., Tang, Z. & Zeng, G., 2011. A gis-based spatial multi-criteria approach for
 973 flood risk assessment in the dongting lake region, hunan, central china. *Water resources*
 974 *management*, 25 (13), 3465-3484.
- 975 Warpo, 2018. National water resources database (nwrdb). . Dhaka, Bangladesh.: Water
 976 Resources Planning Organization (WARPO).
- 977 Worldpop, 2020. The spatial distribution of population in 2020, bangladesh University of
 978 Southampton.
- 979 Youden, W.J., 1950. Index for rating diagnostic tests. *Cancer*, 3 (1), 32-35.
- 980 Zadeh, L.A., 1996. Fuzzy sets. *Fuzzy sets, fuzzy logic, and fuzzy systems: Selected papers by*
 981 *lotfi a zadeh*. World Scientific, 394-432.
- 982 Zou, Q., Zhou, J., Zhou, C., Song, L. & Guo, J., 2013. Comprehensive flood risk assessment
 983 based on set pair analysis-variable fuzzy sets model and fuzzy ahp. *Stochastic*
 984 *Environmental Research and Risk Assessment*, 27 (2), 525-546.

985